



universität  
wien

# DIPLOMARBEIT

Titel der Diplomarbeit

## Blood-brain barrier permeability of six 3-hydroxypyridin-4-ones *in vitro*

Verfasserin

Katharina Brandner

angestrebter akademischer Grad

Magistra der Pharmazie (Mag.pharm.)

Wien, im März 2012

Studienkennzahl lt. Studienblatt:

A 449

Studienrichtung lt. Studienblatt:

Pharmazie

Betreuer:

O. Univ.-Prof. Dipl.-Ing. Mag. Dr. Christian Noe



## **Acknowledgements**

First and foremost, I would like to express my gratitude to my supervisors at King's College London, Prof. Dr. Robert Hider and Dr. Jane Preston as well as my supervisor at the University of Vienna, Prof. Dr. Christian Noe, for giving me the opportunity to work on this project.

Furthermore, I would like to thank Ana Georgian for introducing me to primary cell culture and helping me with any problems I encountered. I am grateful to Abdu Soltani, who always tried to answer my questions about HPLC. Most importantly, I thank Magda, Elleonora, Paolo, Francesca, Gian, Abhi and Franzi for always cheering me up when things didn't go as planned in the lab and for making my stay in London an absolutely unforgettable experience.

Above all, I want to express my deep gratitude for my parents, who always supported me throughout my time at the university. In addition, I thank all my friends, especially Anna, Irene and Manon, who made studying pharmacy so enjoyable.

At last, I owe a special thank you to Dominik, for his love and constant support through the last years.



---

## Table of contents

<b>1</b>	<b>INTRODUCTION .....</b>	<b>1</b>
<b>1.1</b>	<b>The blood-brain barrier .....</b>	<b>1</b>
1.1.1	Cell types at the BBB - the neurovascular unit .....	1
1.1.2	Intercellular junctions - the BBB as a physical barrier .....	3
1.1.3	The BBB as a metabolic barrier .....	6
1.1.4	Transport across the BBB - the BBB as a transport barrier .....	6
<b>1.2</b>	<b>Models to measure and predict BBB permeability .....</b>	<b>9</b>
1.2.1	<i>In vivo</i> .....	9
1.2.2	<i>In vitro</i> .....	10
1.2.2.1	Cells from noncerebral origin .....	10
1.2.2.2	Brain endothelial cells .....	11
1.2.3	<i>In silico</i> .....	12
<b>1.3</b>	<b>Iron, oxidative stress and neurodegeneration.....</b>	<b>13</b>
1.3.1	Iron .....	13
1.3.2	Oxidative stress .....	14
1.3.3	Neurodegeneration and oxidative stress.....	15
1.3.3.1	Alzheimer's disease .....	15
1.3.3.2	Parkinson's disease .....	16
1.3.3.3	Friedreich's Ataxia.....	17
1.3.4	Iron chelation as a therapeutic strategy .....	17
1.3.4.1	Hydroxypyridinones .....	19
<b>1.4</b>	<b>Aims and objectives.....</b>	<b>20</b>
<b>2</b>	<b>MATERIALS AND METHODS .....</b>	<b>21</b>
<b>2.1</b>	<b>Materials .....</b>	<b>21</b>
2.1.1	Chemicals .....	21
2.1.2	Cells.....	21
2.1.3	Analytical apparatus .....	21
<b>2.2</b>	<b>Methods.....</b>	<b>23</b>
2.2.1	Cell culture .....	23

---

2.2.1.1	Cerebral microvessel endothelial cell isolation.....	23
2.2.1.2	Defrosting PBECs .....	23
2.2.1.3	Passaging PBECs .....	24
2.2.1.4	Primary astrocytes .....	25
2.2.1.5	C6 glioblastoma .....	26
2.2.2	Assessing cell viability.....	26
2.2.2.1	Cytotoxicity assay .....	26
2.2.2.2	BCA protein assay.....	26
2.2.2.3	Calculating overall cell viability .....	27
2.2.3	Permeability assay.....	27
2.2.3.1	Culture conditions .....	28
2.2.3.2	Enhancing barrier properties .....	28
2.2.3.3	Determining the quality of the barrier.....	29
2.2.3.4	Experiment protocol.....	30
2.2.3.5	Correcting HPO transfer .....	31
2.2.3.6	Calculating intracellular accumulation .....	31
2.2.4	HPLC.....	31
2.2.5	Statistical analysis .....	32
<b>3</b>	<b>RESULTS.....</b>	<b>33</b>
<b>3.1</b>	<b>Viability .....</b>	<b>33</b>
3.1.1	CP20.....	33
3.1.2	HPO viability .....	34
3.1.2.1	Viability after 20min incubation .....	35
3.1.2.2	Viability after 2 hour incubation .....	36
<b>3.2</b>	<b>CP20 time-dependent transport.....</b>	<b>37</b>
<b>3.3</b>	<b>Relationship between TEER and sodium fluorescein permeability .....</b>	<b>40</b>
<b>3.4</b>	<b>Influence of the culture condition .....</b>	<b>41</b>
3.4.1	Influence on TEER.....	41
3.4.2	Influence on sodium fluorescein permeability .....	42
<b>3.5</b>	<b>Permeability assay.....</b>	<b>43</b>
3.5.1	HPO transfer.....	43
3.5.2	<i>In vivo – in vitro</i> correlation .....	44

---

3.5.3	Intracellular accumulation.....	45
3.5.4	Transfer + intracellular accumulation and <i>in vivo</i> – <i>in vitro</i> correlation.....	46
3.5.5	Permeability vs. logD <sub>7.4</sub> and MW .....	47
<b>3.6</b>	<b>HPLC.....</b>	<b>49</b>
<b>4</b>	<b>DISCUSSION.....</b>	<b>50</b>
4.1	<i>In vitro</i> system.....	50
4.2	<i>In vivo</i> – <i>in vitro</i> correlation.....	53
4.3	Influence of structural features on BBB permeability .....	54
4.4	Toxicity and neuroprotection .....	56
4.5	Clinical use.....	57
<b>5</b>	<b>ABSTRACT .....</b>	<b>58</b>
<b>6</b>	<b>ZUSAMMENFASSUNG .....</b>	<b>59</b>
<b>7</b>	<b>REFERENCES .....</b>	<b>60</b>
<b>8</b>	<b>CURRICULUM VITAE.....</b>	<b>67</b>
<b>9</b>	<b>APPENDIX.....</b>	<b>68</b>
9.1	HPO standard curves.....	68
9.2	HPLC chromatograms.....	71
9.3	YMF 29 mass spectrometry .....	74

## List of figures

Figure 1: Schematic representation of the constituents of the neurovascular unit (modified from Abbott et al., 2006).....	2
Figure 2: Schematic representation of the structure of the tight junctions at the blood-brain barrier (from Abbott et al., 2010).....	4
Figure 3: Schematic representation of transport across the blood-brain barrier.....	7
Figure 4: Schematic representation of iron-ligand complexes (from Gaeta and Hider, 2005) .....	17
Figure 5: Confluent PBEC monolayer (from Bobilya et al., 1995).....	24
Figure 6: Schematic representation of a Transwell® insert used for the <i>in vitro</i> permeability assay.....	28
Figure 7: Schematic representation of a Transwell® insert with PBECs grown in non-contact co-culture with C6 glioblastoma .....	28
Figure 8: Schematic representation of the TEER measurement with copstick electrodes (from Cardoso et al., 2010).....	29
Figure 9: Protein content per well in µg, determined after performing the BCA assay on PBECs incubated with CP20 for 2 hours.....	33
Figure 10: Absorbance measured at 540nm, after the MTT assay was conducted on PBECs incubated with CP20 for 2 hours.....	33
Figure 11: PBEC overall viability after incubation with CP20 for 2 hours, expressed in absorbance per µg protein.....	34
Figure 12: Protein content per well in µg, determined after performing the BCA assay on PBECs incubated with 800µM HPO for 20min.....	35
Figure 13: Absorbance measured at 540nm, after the MTT assay was conducted on PBECs incubated with 800µM HPO for 20min.....	35
Figure 14: PBEC overall viability, expressed in absorbance per µg protein, after incubation with 800µM HPO for 20min.....	35
Figure 15: Absorbance measured at 540nm, after the MTT assay was conducted on PBECs incubated with 800µM HPO for 2 hours.....	36
Figure 16: Protein content per well in µg, determined after performing the BCA assay on PBECs incubated with 800µM HPO for 2 hours.....	36
Figure 17: Overall viability, expressed in absorbance per µg protein for PBECs incubated with 800µM HPO for 2 hours.....	37
Figure 18: Time dependent transfer of 800µM CP20 across the PBEC monolayer.....	38
Figure 19: Transfer of CP 20 expressed in mg, for the 3 experimental conditions (explanation in the text) after 20min, 40min and 60min.....	39
Figure 20: Relationship between TEER and sodium fluorescein transfer with fitted curves for each of the 3 culture conditions and for the pooled data from all culture conditions (n=78).....	40



---

Figure 21: Electrical resistance over the PBEC monolayer expressed in $\Omega\cdot\text{cm}^2$ , shown for each of the 3 culture conditions: .....	41
Figure 22: Sodium fluorescein permeability in percent, shown for each of the 3 culture conditions:.....	42
Figure 23: HPO overall transfer in percent across the PBEC monolayer (further explanation in the text).....	43
Figure 24: HPO transfer across the PBEC monolayer corrected for paracellular transport, expressed in percent (further explanation in the text).....	44
Figure 25: Correlation between <i>in vitro</i> and <i>in vivo</i> HPO blood-brain barrier permeability. ....	45
Figure 26: Calculated intracellular HPO accumulation in percent. ....	45
Figure 27: Correlation between calculated intracellular accumulation and $\log D_{7.4}$ .....	45
Figure 28: Combined values of HPO transfer and calculated intracellular accumulation in percent.....	46
Figure 29: Correlation between <i>in vitro</i> (transfer + intracellular accumulation) and <i>in vivo</i> HPO transfer.....	47
Figure 30: Molecular weight (MW) plotted against <i>in vitro</i> HPO transfer added to intracellular accumulation (expressed in percent). ....	48
Figure 31: Molecular weight (MW) plotted against <i>in vivo</i> HPO transfer (expressed in percent). ....	48
Figure 32: $\log D_{7.4}$ plotted against <i>in vitro</i> HPO transfer added to intracellular accumulation (expressed in percent).....	48
Figure 33: $\log D_{7.4}$ plotted against <i>in vivo</i> HPO transfer (expressed in percent). ....	48
Figure 34: Structure of YMF 8, YMF 16, YMF 24 and YMF 25. Intramolecular hydrogen bonds shown for YMF 8 and YMF 24 .....	54
Figure 35: $\log D_{7.4}$ plotted against HPO <i>in vitro</i> transfer added to intracellular accumulation (expressed in percent). The arrow points out the dot that represents YMF 29.....	55
Figure 36: $\log D_{7.4}$ plotted against HPO <i>in vivo</i> permeability (expressed in percent). The arrow points out the dot that represents YMF 29.....	55
Figure 37 Structure and intramolecular hydrogen bonds of YMF 29 .....	56
Figure 38: Standard curve CP20 .....	68
Figure 39: Standard curve YMF 8 .....	68
Figure 40: Standard curve YMF 16 .....	69
Figure 41: Standard curve YMF 24 .....	69
Figure 42: Standard curve YMF 25 .....	70
Figure 43: Standard curve YMF 29 .....	70
Figure 44: HPLC chromatogram CP20 (1mM), 100 $\mu\text{L}$ injection.....	71
Figure 45: HPLC chromatogram YMF 8 (1mM), 100 $\mu\text{L}$ injection .....	71

---

Figure 46: HPLC chromatogram YMF 16 (1mM), 100 $\mu$ L injection .....	72
Figure 47: HPLC chromatogram YMF 24 (1mM), 100 $\mu$ L injection .....	72
Figure 48: HPLC chromatogram YMF 25 (1mM), 100 $\mu$ L injection .....	73
Figure 49: HPLC chromatogram YMF 29 (1mM), 100 $\mu$ L injection .....	73
Figure 50: ESI MS(+ve) of YMF 29 (MW 267; YMF 29 – HBr: MW 187), 20 $\mu$ L of sample diluted to 1mL with 0.1% FA in 50% MeOH .....	74

## List of formulas

Formula 1: deferiprone .....	19
Formula 2: sodium fluorescein .....	30

## List of tables

Table 1: Structure, molecular weight (MW) and $\log D_{7.4}$ of the HPOs used in this study	222
---	-----

## List of schemes

Scheme 1: Fenton reaction .....	15
---------------------------------	----

## List of abbreviations

+ve – positive  
ABC - ATP-binding cassette  
ACM – astrocyte-conditioned media  
AD - Alzheimer's disease  
AJ - adherens junctions  
AMT - absorptive mediated transcytosis  
ANG1 - angiopoetin 1  
APP - amyloid precursor protein  
ATP – adenosine triphosphate  
AUC – area under the curve  
A $\beta$  – amyloid  $\beta$   
BBB – blood-brain barrier  
BCA - 2-bicinchoninic acid  
BCRP - breast cancer resistance protein  
bFGF - basic fibroblast growth factor  
BPDS - bovine plasma derived serum  
BSA - bovine serum albumin  
C6 co – co-culture with C6 glioblastoma  
CAM - cell adhesion molecules  
cAMP – cyclic adenosine monophosphate  
CASK - Ca<sup>2+</sup> dependent serine protein kinase  
CNS – central nervous system  
CP20 - deferiprone  
CPT-cAMP - 8-4-chlorophenylthio-cAMP  
DMEM - Dulbecco's modified eagle medium  
DMSO – dimethyl sulfoxide  
DNA – deoxyribonucleic acid  
e.g. - *exempli gratia*  
EAAT - excitatory amino acid transporter  
EDTA - Ethylenediaminetetraacetic acid  
eNOS - endothelial nitric oxide synthase  
ESI – electron spray ionisation  
FCS - fetal calf serum  
GDNF - glial-derived neurotrophic factor  
GLUT – glucose transporter  
h - hour  
HBr – hydrogen bromide  
HBSS – Hank's balanced salt solution  
HCl – hydrochloric acid  
HEPES - 4-(2-hydroxyethyl)-1-piperazineethanesulfonic acid  
HPLC - High-performance liquid chromatography  
HPO – 3-hydroxypyridin-4-one  
IgG – immunoglobulin G  
IRE - iron responsive element  
IRP - iron regulatory protein  
JACOP - junction-associated coiled-coil protein  
JAM - junction associated molecules

kDa - Kilodalton  
LAT1 - large neutral amino acid transporter  
M – molar  
MAPK - mitogen-activated protein kinase family  
MDR 1 gene – multi drug resistance 1 gene  
MEM – Minimal essential medium eagle  
MeOH – methanol  
min – minute  
mono – monoculture  
MRI - magnetic resonance imaging  
mRNA – messenger ribonucleic acid  
MRP - multidrug resistance associated protein  
MS - mass spectrometry  
MS – mass spectrometry  
MTT - 3-(4,5-dimethylthiazol-2-yl)-2,5-diphenyl tetrazolium bromide  
MW - molecular weight  
NVU - neurovascular unit  
OAT - organic anionic transporter  
OCT - organic cationic transporter  
PBEC - primary porcine brain endothelial cells  
PD - Parkinson's disease  
PECAM - platelet-endothelial cell adhesion molecule  
PET - positron emission tomography  
P-gp – P-glycoprotein  
PSA – polar surface area  
RMT - receptor-mediated transcytosis  
RO - RO-20-1724  
ROS – reactive oxygen species  
rpm – rotations per minute  
s – second  
SLC - solute carrier transporter  
TEER - transendothelial electrical resistance  
TGF $\beta$  - transforming growth factor  $\beta$   
TJ – tight junctions  
TNF $\alpha$  – tumor necrosis factor  $\alpha$   
v - volume  
VE cadherin - vascular endothelial cadherin  
ZO - zonula occludens

# 1 INTRODUCTION

## 1.1 The blood-brain barrier

The blood-brain barrier (BBB) is formed by microvascular endothelial cells to separate blood from brain parenchyma (Abbott et al., 2010). It is the largest interface between the central nervous system (CNS) and the periphery, covering 12-18m<sup>2</sup> total area of exchange between the circulating blood and the brain in an average human adult brain (Abbott et al., 2010).

Acting as a physical, metabolic and transport barrier, the BBB not only preserves the homeostatic environment essential for neurons by providing a stable ionic composition necessary for optimal neuronal function, but also ensures sufficient nutrient supply and the separation of neurotransmitter pools between the central and the peripheral nervous system (Abbott et al., 2010; Bernacki et al., 2008). Moreover, the BBB protects the brain from potentially neurotoxic substances of endogenous or xenobiotic origin (Abbott et al., 2010).

### 1.1.1 Cell types at the BBB - the neurovascular unit

The BBB is primarily formed by the endothelial cells of cerebral vessels. These endothelial cells differ in their characteristics from endothelial cells in other organs, since they lack fenestration, show low transcytotic activity and the presence of tight junctions (TJ) (Hawkins and Davis, 2005). The surface of the endothelial cells is negatively charged, facilitating transport of positively charged molecules. In addition, endothelial cells in the BBB have a greater number of mitochondria (Cardoso et al., 2010; Abbott et al., 2010; Persidsky et al., 2006). The higher number of mitochondria elevates the energy potential of the endothelial cells providing the energy required to actively transport nutrients into the brain and potentially harmful substances out of the brain (Persidsky et al., 2006).

However, the regulation of the barrier characteristics is not entirely determined by the endothelial cells, but rather is an interaction of different cells types present at the interface of blood and brain, suggesting that these cells form a functional unit that is referred to as the neurovascular unit (NVU). The NVU consists of the endothelial cells, astrocytic glia cells, pericytes, the basement membrane and the neurons (Hawkins and Davis, 2005;

Cardoso et al., 2010) (Figure 1).

Astrocytes are glial cells whose end-feet envelop the walls of the endothelium. This close contact enables them to be involved in the modulation and induction of BBB properties (Abbott, 2002), while gap junctions between neighbouring astrocyte processes permit communication with other astrocytes (Abbott et al., 2006). *In vitro* studies have shown that astrocytes play an important role in many processes, for example up-regulating enzymes, tight junctions and the polarized expression of transporters like P-glycoprotein (P-gp) and glucose transporter GLUT-1 (Abbott et al., 2006). Furthermore, astrocytes contribute to the specific ionic, amino acid and water homeostasis required for proper brain function (Abbott et al., 2006).

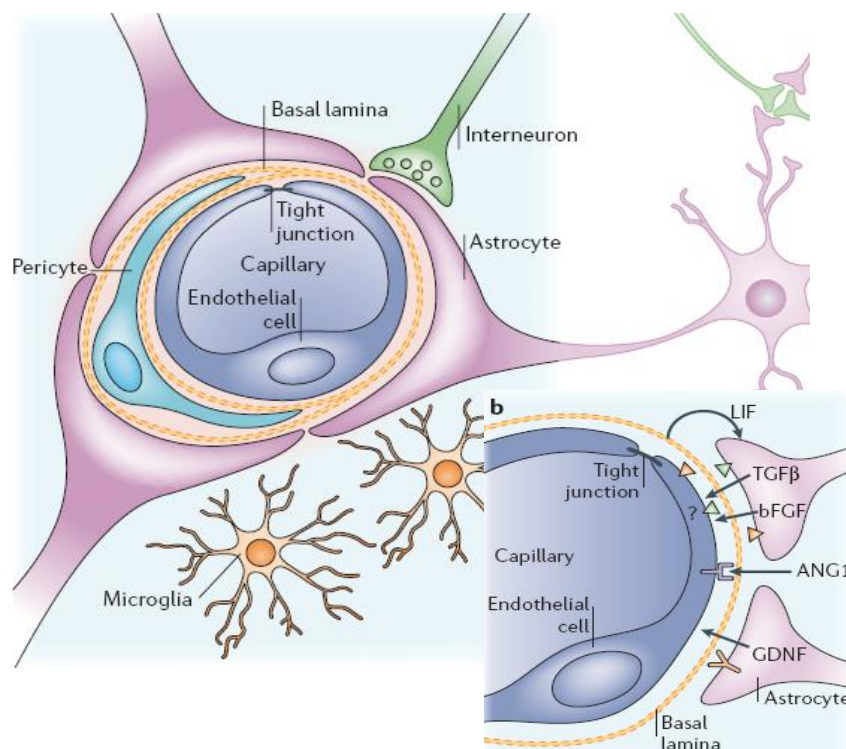


**Figure 1: Schematic representation of the constituents of the neurovascular unit (modified from Abbott et al., 2006)**

Research has shown that areas of the endothelium that lack astrocyte envelopment, still express specific BBB characteristics leading to the suggestion that astrocytes are able to secrete soluble factors (Cardoso et al., 2010). These factors include transforming growth factor  $\beta$  (TGF $\beta$ ), glial-derived neurotrophic factor (GDNF), basic fibroblast growth factor (bFGF) and angiopoetin 1 (ANG1), which have all been shown to improve BBB properties *in vitro* (Abbott et al., 2006).

Pericytes are another constituent of the NVU. Pericytes are vascular smooth muscle cells that are spread discontinuously along the capillaries and in part surround the endothelium (Abbott et al., 2010). Via their cellular projections and gap junctions, pericytes are in close contact with the endothelial cells *in vivo* and have been shown to induce BBB properties *in vitro* such as increased tightness of the barrier and up-regulation of P-gp (Nakagawa et al., 2007). Moreover, pericytes have been found to migrate away from microvessels as a consequence of hypoxia or traumatic brain injury, both associated with barrier disruption, which further points to their involvement in maintaining barrier function (Cardoso et al., 2010; Persidsky et al., 2006).

The basement membrane, that engulfs pericytes and endothelial cells, consists of collagen type IV, elastin, fibrillin, laminin and fibronectin in addition to cell adhesion molecules (CAM) and signalling proteins (Carvey et al., 2009). Endothelial cells, pericytes and astrocytes are all involved in the synthesis of this complex matrix, which acts as an anchor keeping these cells in place. Furthermore, the basement membrane is involved in the regulation of cellular functions and TJ expression through the activation of signalling proteins on the surface of the endothelial cells (Carvey et al., 2009; Hawkins and Davis, 2005). Thus, alterations or disruption of the basement membrane have been shown to be connected with loss of BBB integrity in pathological conditions (Hawkins and Davis, 2005).

### **1.1.2 Intercellular junctions - the BBB as a physical barrier**

The presence of intercellular junctions like tight junctions (TJ) and adherens junctions (AJ) give the BBB its characteristic properties, considering that these structures not only severely restrict paracellular transport of compounds circulating in the blood from entering the brain (physical barrier) but also separate the apical from the basal domain, necessary for the polarized expression of transporters (transport barrier) (Abbott et al., 2006).

The TJ are formed by 3 transmembrane protein families: occludin, claudin and junction associated molecules (JAM). These proteins interact with cytoplasmic proteins like zonula occludens proteins (ZO), linking the TJ proteins to the components of the cytoskeleton (Weiss et al., 2009; Abbott et al., 2010) (Figure 2).

Occludin is a 65 kDa protein with 4 transmembranous domains, 2 extracellular loops and

the N- and C-terminal domains both situated in the cytoplasm. The extracellular loops enable occludin to span the intracellular cleft (Hawkins and Davis, 2005; Persidsky et al., 2006) and this consequently contributes to the formation of tight junction and regulation of paracellular permeability (Persidsky et al., 2006). However, in experiments with knock-out mice it was demonstrated that occludin is not essential for TJ formation, even though decreased expression of occludin is connected to loss of barrier integrity in pathological conditions (Hawkins and Davis, 2005). Thus, it is believed that occludin enhances the restrictiveness of the TJ, yet claudins are the components responsible for the establishment of the barrier properties (Wolburg and Lippoldt, 2002; Hawkins and Davis, 2005).

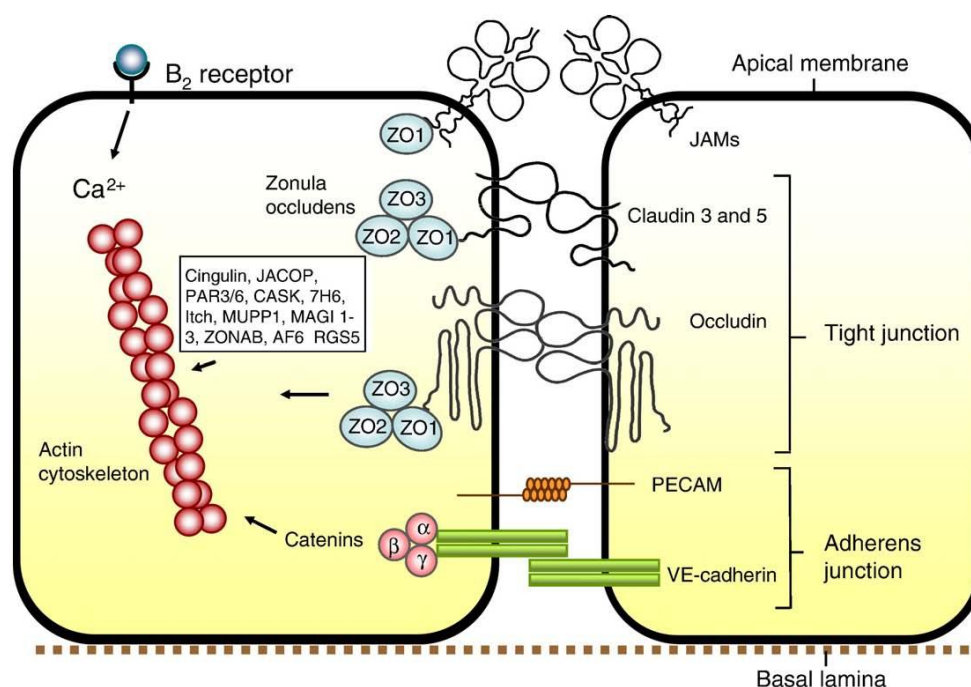


**Figure 2: Schematic representation of the structure of the tight junctions at the blood-brain barrier (from Abbott et al., 2010)**

Claudins are 20-24 kDa proteins, that like occludin, have 4 transmembranous domains and 2 extracellular loops (Hawkins and Davis, 2005; Abbott et al., 2006), but do not share any sequence homology with occludin (Wolburg and Lippoldt, 2002). The extracellular loops mediate homophilic and heterophilic interaction between adjacent cells (Hawkins and Davis, 2005). These interactions are responsible for the severe restriction of movement for water-soluble molecules via the paracellular pathway, forcing the molecules to move through the membranes and the cytosol (Bernacki et al., 2008).



Both claudin and occludin bind to accessory proteins such as the zonula occludens proteins (ZO 1-3) to connect the transmembranous TJ proteins with the actin cytoskeleton (Abbott et al., 2006). These scaffolding proteins are also responsible for the recruitment of various signalling proteins and transcription factors to the TJ (Terry et al., 2010; Abbott et al., 2006). ZOs together with  $\text{Ca}^{2+}$  dependent serine protein kinase (CASK) are considered first order adaptor proteins and second order adaptor proteins include cingulin as well as junction-associated coiled-coil protein (JACOP) (Abbott et al., 2006). In addition to the presence of occludin and claudin at the TJ of the BBB, junction adhesion molecules (JAMs) also contribute to the formation of the TJ (Abbott et al., 2006) as well as being involved in leukocyte migration (Cardoso et al., 2010). JAMs belong to the IgG superfamily and in contrast to occludin and claudin have only one transmembranous domain (Persidsky et al., 2006; Bernacki et al., 2008).

Below the TJ, adherens junctions (AJ) are formed to further stabilize cell-cell interactions and to give structural support (Abbott et al., 2006). AJ are believed to play a role in the maintenance of the barrier function, since AJ disruption can lead to increased permeability (Abbott et al., 2010). The AJ are composed of the transmembranous proteins vascular endothelial cadherin (VE cadherin) and platelet-endothelial cell adhesion molecule (PECAM), which are linked to the cytoskeleton via the scaffolding proteins of the catenin family (alpha, beta and gamma) and the protein desmoplakin is also involved in the process (Abbott et al., 2006).

However, the TJ must not be regarded as a static element but as a dynamic structure that can be modulated (e.g. phosphorylation of TJ proteins) according to different stimuli like oxidative stress, vasogenic agents and inflammatory mediators (Cardoso et al., 2010). TJs can be opened or tightened through various pathways including protein kinases, members of the mitogen-activated protein kinase family (MAPK), endothelial nitric oxide synthase (eNOS), G-proteins and signalling pathways involving  $\text{Ca}^{2+}$  as a second messenger (Cardoso et al., 2010). The signalling at the TJs is a bi-directional process with the signal forwarded from the inside of the endothelial cells to the TJ proteins as well as TJ proteins transmitting information back to the endothelial cells. This results in the regulation of gene expression leading to cellular responses like proliferation and differentiation (Terry et al., 2010).

### **1.1.3 The BBB as a metabolic barrier**

The expression of intra- and extracellular enzymes at the BBB is responsible for its role as a metabolic barrier and are produced by both endothelial and astrocytic cells. Enzyme concentrations are high, when compared to noncerebral endothelial cells (Persidsky et al., 2006) and include monoamine oxidase, gamma-glutamyl transpeptidase, alkaline phosphatase, cytochrome P450 enzymes and several other peptidases and nucleotidases (Cecchelli et al., 2007; Abbott et al., 2006).

### **1.1.4 Transport across the BBB - the BBB as a transport barrier**

Depending on its characteristics, a molecule can enter the brain via several different routes of transport across the BBB (Figure 3).

Due to the restrictive nature of the tight junction at the BBB, transport across the BBB is limited especially for water-soluble molecules, consequently isolating the brain from essential nutrients like glucose and amino acids (Abbott et al., 2010). In order to ensure adequate brain nutrition, specific solute carrier transporters (SLC) are expressed by the endothelial cells to facilitate their entry, since these polar nutrients cannot passively diffuse through the cell membranes (Abbott et al., 2010). Their expression can be either at the luminal and/ or at the abluminal side, regulating transport across the endothelium either into or out of the brain respectively (Abbott et al., 2010). Over 40 different families of SLC have been indentified so far (Eyal et al., 2009). Among these are several amino acid transporters like the LAT1 (for large neutral amino acids), as well as the organic anionic and cationic transporters (OAT, OCT), the glutamate transporter EAAT (excitatory amino acid transporter) and several transporters for nucleosides and nucleotides (Abbott et al., 2006; Bernacki et al., 2008; Eyal et al., 2009). Importantly, there is also a high expression of the glucose transporter GLUT-1 to supply glucose to the brain and its expression is modulated according to metabolic demands (Xiuli et al., 2003).

Oxygen and carbon dioxide on the other hand can diffuse freely through the membranes along their concentration gradients, hence the oxygen supply and the carbon dioxide removal is entirely dependent on blood flow (Abbott et al., 2010).

Macromolecules such as peptides and proteins take the route of receptor-mediated (RMT) or absorptive mediated transcytosis (AMT) across the BBB (Abbott et al., 2010). In the case of RMT, after binding to the receptor the macromolecule is internalised with its receptor, transferred across the cell in a vesicle, and exocytosed on the abluminal membrane, during which it is presumed that there is a dissociation of the macromolecule from its receptor (Abbott et al., 2010). On the other hand, AMT requires a positively charged macromolecule interacting with the negatively charged surface of the membrane, which triggers the endocytotic process. Substrates for RMT include insulin, transferrin, lipoproteins, IgG and TNF $\alpha$ , whereas cationised albumin and other plasma proteins are examples for transport via AMT (Abbott et al., 2010).

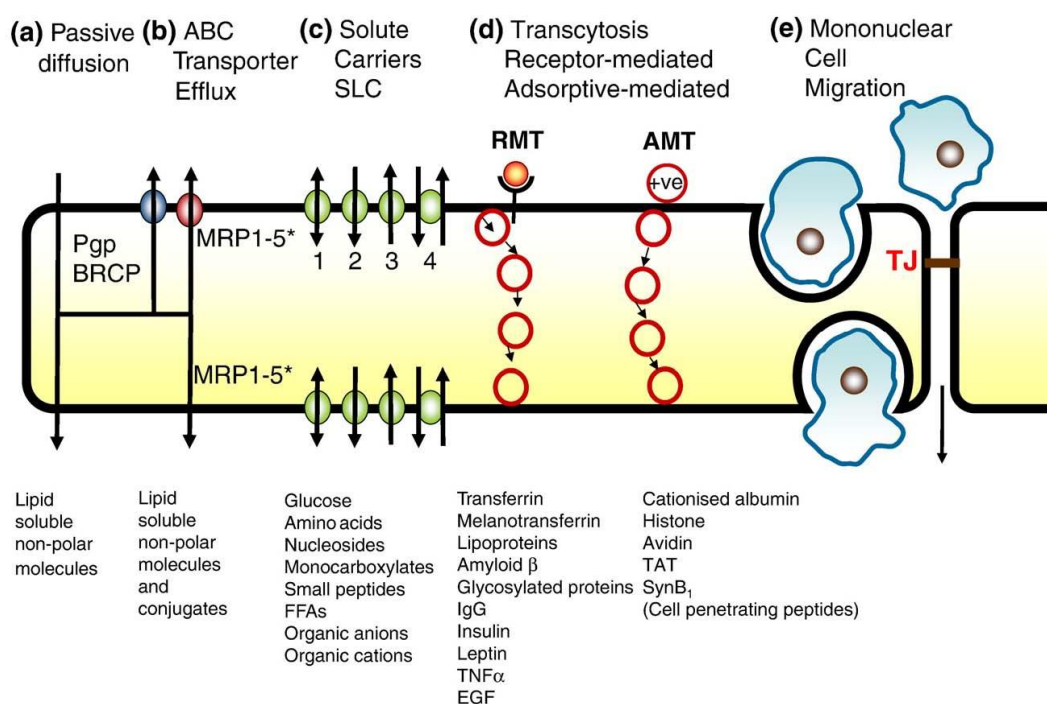


**Figure 3: Schematic representation of transport across the blood-brain barrier (from Abbott et al., 2010)**

Lipid-soluble molecules, in contrast to macromolecules and water-soluble molecules can in principle diffuse freely across the BBB along their concentration gradient. The more lipid-soluble a compound is, the more likely it is to enter the brain successfully. However, their ability to do so is often lower than expected from their physicochemical properties due to the presence of efflux pumps at the BBB, known as ABC Transporters (ATP-binding Cassette) (Abbott et al., 2010).

ABC transporters utilize energy supplied by ATP hydrolysis to actively efflux potentially neurotoxic substances, of either endogenous or xenobiotic origin, out of the brain (Löscher and Potschka 2005a). A total of 48 families of ABC transporters divided into 7 subfamilies are known in humans of which P-glycoprotein (P-gp, ABC B1) is the best characterized (Begley, 2004; Leslie et al., 2005). P-gp was first discovered in association with drug resistance of tumour cells (Eyal et al., 2009; Löscher and Potschka, 2005b) and is a 170 kDa glycoprotein with 12 transmembranous domains and 2 intracellular binding sites for ATP (Begley, 2004). P-gp is expressed at the luminal side of the BBB (Begley 2004) and substrates include cytostatics (e.g. anthracyclines, vinca alkaloids, and taxanes), antiepileptic drugs (e.g. phenobarbital and carbamazepine) and protease inhibitors (e.g. indinavir and nelfinavir) (Löscher and Potschka, 2005b).

Other members of the ABC transporter family include the multidrug resistance associated proteins (MRPs, ABC C family), which can be located either in the luminal or abluminal membrane of the endothelial cells (Eyal et al., 2009; Begley, 2004, Löscher and Potschka 2005a) and the breast cancer resistance protein (BCRP), which is located in the luminal membrane (Eyal et al., 2009). Contrary to P-gp, MRPs favour anionic compounds and neutral compounds that are conjugated to glutathione, glucuronate or sulphate as substrates (Borst et al., 2000). An overlap with substrates for P-gp exists as well as there is a partial overlap for BCRP and P-gp substrates (Begley, 2004; Löscher and Potschka 2005b; Eyal et al., 2009).

The ability of ABC transporters to efflux a wide range of structurally and functionally diverse compounds out of the brain presents a major problem for the effective delivery of drugs into the CNS. This has led to the idea of modulating the BBB by using inhibitors for efflux pumps, like verapamil or cyclosporin A for P-gp (Löscher and Potschka, 2005b). However, the risks involved in modulating these efflux pumps must clearly be kept in mind (Löscher and Potschka, 2005b).

## 1.2 Models to measure and predict BBB permeability

In order to effectively treat a disease, a drug is required to reach the desired pharmacological target. In the case of a CNS related disease, the drug must be able to get into the brain, therefore it is necessary to cross the blood-brain barrier (BBB). Models to assess BBB permeability can be categorized as *in vivo*, *in vitro* and *in silico* models and each have their strengths and limitations (Mensch et al., 2009).

### 1.2.1 *In vivo*

*In vivo* methods still provide the most reliable information for testing and validating other models (Abbott, 2004), even though the techniques involved are both cost and labour intensive. Brain uptake can be measured according to two methodological approaches: equilibrium state based approaches to measure the extent of brain penetration and the brain/plasma ratio or approaches based on kinetic parameters, which aim to determine the rate of brain penetration and the permeability  $\times$  surface product (Mensch et al., 2009). For this purpose either non-invasive or invasive techniques can be applied.

Non-invasive techniques include PET (positron emission tomography) and MRI (magnetic resonance imaging), which can also be applied in humans and allow individual time course studies for brain uptake. These methods are highly sensitive, but since their use is expensive and the preparation and stability of the tracer substances can present a difficulty, these techniques are not used in routine drug screening (Mensch et al., 2009).

Intravenous injection, brain uptake index and *in situ* brain perfusion are invasive techniques to measure brain uptake and involve the injection of the test compound, which is usually radiolabelled. In contrast to the intravenous injection, the brain uptake index technique uses a single injection directly into the carotid artery of the animal, hence avoiding systemic recirculation. The animal is decapitated after 15s and the amount of test compound in the brain is determined (Mensch et al., 2009; Bickel, 2005). The *in situ* brain perfusion uses longer perfusion times, between 60s and 60min, which makes it more sensitive and additionally the flow rate as well as the ionic composition of the perfusate can be adjusted (Bickel, 2005; Mensch et al., 2009). The perfusate is injected into the external carotid artery, which has been ligated with all the branches of the internal carotid artery prior to injection. This set up eliminates the disadvantages of the brain uptake index as it limits systemic circulation and metabolism (Mensch et al., 2009).

Though intracerebral microdialysis is also an invasive technique it can be performed on live animals, which is a great advantage. A probe with a semipermeable membrane is implanted into the brain of the animal and perfused with a physiological solution. The test compound is administered orally, subcutaneously or intravenously and, if able to enter the brain, can diffuse into the perfusate along its concentration gradient, where the concentration can be determined. Nevertheless, the implantation of the probe can damage the BBB and compromise its functionality (Mensch et al., 2009).

### **1.2.2 *In vitro***

*In vitro* models are simplifications of the *in vivo* situation, but are usually less labour intensive compared to *in vivo* models. An *in vitro* model should be robust, reproducible and most importantly needs to mimic the *in vivo* conditions as closely as possible. This should be in regard to the specific characteristics of the BBB, such as its morphology, presence of tight junctions (TJ) and expression of transporters and enzymes (Cecchelli et al., 2007).

To assess the quality of the model two factors are usually referred to: the transendothelial electrical resistance (TEER) and the permeability of tracer substances. The TEER presents a good indication of the integrity and tightness of the barrier to small ions and the measurements can be easily and quickly carried out (Gumbleton and Audus, 2001). While TEER measurements alone might only provide limited information on the barrier properties, together with the permeability measurements of tracer substances it is possible to determine the development of a restrictive barrier (Gumbleton and Audus, 2001). These tracer substances must not be substrates for either uptake or efflux transporters and are fluorescent- or radiolabelled. Sodium fluorescein, fluorescent-labelled dextrans and radiolabelled sucrose, inulin and mannitol are most commonly used (Deli et al., 2005).

Several different *in vitro* models, originating from different species and tissues, have been studied and discussed in the literature as potential BBB models, but there is yet no “gold standard” for a BBB *in vitro* model, hence the choice of the model depends on the study question (Abbott, 2004).

#### **1.2.2.1 Cells from noncerebral origin**

Cell lines from noncerebral origin have been tested to serve as surrogate BBB models

(Abbott, 2004), but usually fail due to insufficient barrier properties (Mensch et al., 2009). The MDCK (Madin-Darby-Canine Kidney) shows high TEER values and low sucrose permeability and can furthermore be transfected with the MDR1 gene to achieve the polarized P-gp expression (Mensch et al., 2009). In spite of this, the MDCK cell line differs in gene expression, cell morphology and cell-cell junctions from brain endothelial cells (Cecchelli et al., 2007). The ECV304 cell line, which originates from a bladder carcinoma and shows epithelial and endothelial properties, and the Caco-2 cell line, which is derived from a human colon adenoma and is widely used in the industry as a well-established *in vitro* model for intestinal absorption, have both been dismissed as suitable BBB models for similar reasons (Cecchelli et al., 2007; Mensch et al., 2009).

### **1.2.2.2 Brain endothelial cells**

#### 1.2.2.2.1 Primary and low-passage endothelial cells

Endothelial cells from brain microvessels can be isolated and cultured, where they are able to form monolayers and allow the performance of experiments (Abbott, 2004). Since it is difficult to obtain human brain tissue due to ethical constrictions and because the tissue received cannot always be regarded as healthy (surgical material or from autopsies), a wide range of different animals are used to obtain primary brain endothelial cells (Deli et al., 2005; Wilhelm et al., 2011). Although the availability of transgenic rodents like mice and rats is appealing (Deli et al., 2005; Wilhelm et al., 2011), because of their size the yield of endothelial cells from one brain is relatively small (1-2 million/brain) (Gumbleton and Audus, 2001; Mensch et al., 2009). Hence models from bovine or porcine origin are favoured, having a yield of approximately 200 million cells/brain (Mensch et al., 2009).

However, the cultivation of primary brain endothelial cells can lead to a loss of characteristic BBB properties as certain features like transporters and tight junction proteins can be down-regulated or subjected to altered expression (Abbott, 2004). To overcome these limitations, models that resemble the *in vivo* situation more closely have been developed. Astrocytes are anatomically very close to the endothelial cells *in vivo* and have been used to induce barrier properties by up-regulation of tight junction proteins and transporters *in vitro* (Abbott et al., 2006; Deli et al., 2005). Endothelial cells can be cultured either in contact or non-contact co-culture with the astrocytes (Mensch et al., 2009; Cecchelli et al., 2007). Since astrocytes have been shown to secrete soluble factors

to up-regulate barrier characteristics, endothelial cells can also be cultured in astrocyte-conditioned media, which is taken off of separately cultured astrocytes (Abbott et al., 2006; Deli et al., 2005). Therefore either rat astrocytes or the C6 glioma cell line are most commonly used. Both co-culture and treatment with conditioned media has been shown to result in an increase in TEER and a decrease in the permeability of tracer substances and polar solutes (Deli et al., 2005). Recently a triple co-culture model has been developed, which aims to take the influence of pericytes on the BBB *in vivo* into account (Nakawaga et al., 2009).

Additionally, an increase of intracellular cAMP, has been shown to lead to tightening of the barrier resulting in an increase in TEER and a decreasing permeability of tracer substances (Deli et al., 2005; Rubin et al., 1991). Furthermore, when endothelial cells are treated with a phosphodiesterase inhibitor, which prevents the quick metabolism of cAMP, it is possible to reinforce the effect of cAMP treatment (Deli et al., 2005; Rubin et al., 1991). Serum free cultivation and additional treatment with hydrocortisone has also lead to increases in TEER (Deli et al., 2005; Hoheisel et al., 1998).

#### 1.2.2.2.2 Immortalized cell lines

Immortalized cell lines have been developed, aiming to limit some of the disadvantages involved in the cultivation of primary endothelial cells. These disadvantages include the labour intensity of isolating the endothelial cells and the problem of batch-to-batch reproducibility (Mensch et al., 2009; Bickel, 2005). To generate immortalized cell lines, the cells are transformed with viral proteins or genes (Bickel, 2005; Gumbleton and Audus, 2001). In general, these cell lines maintain BBB characteristics, but do not form a sufficiently tight barrier, that allow the performance of permeability studies (Mensch et al., 2009; Gumbleton and Audus, 2001). Well characterized cell lines include the rat RBE4 and the human hCMEC/D3 cell line (Cecchelli et al., 2007).

### 1.2.3 *In silico*

*In silico* models are computer based models, which offer the advantage of being cheaper, less time consuming and high throughput compared to both *in vivo* and *in vitro*, earning them great popularity especially within the pharmaceutical industry. The difficulty lies in the data necessary to generate such models, since experimental protocols differ from study to study and not all data is publicly available. Thus, the quality of the model is



ultimately determined by the data used to build the model (Mensch et al., 2009).

Most models concentrate their prediction on the ability of a compound to enter the brain by passive diffusion, since this is the route for most drugs across the BBB. However, such models do not account for plasma protein binding, metabolism and active influx or efflux (Mensch et al., 2009). Apart from the quality and quantity of the data used for the model, descriptors and the modelling approach further determine the models quality (Mensch et al., 2009). Descriptors are used to define the physicochemical properties of a molecule in an attempt to establish a correlation between the molecular structure and its ability to cross the BBB. These include molecular weight (MW), lipophilicity ( $\log D_{7.4}$ ), ability to form hydrogen bonds and the polar surface area (PSA) (Mensch et al., 2009; Abbott et al., 2010). In general, a compound is predicted to be able to passively diffuse across the BBB if its MW is lower than 450 (Bickel, 2005), its  $\log D$  is 1-3, it does not form more than 6 hydrogen bonds and its PSA is less than  $80\text{\AA}^2$  (Abbott et al., 2010).

Based on the complex structure and interactions at the BBB it is obvious that generating an *in silico* model to accurately predict BBB permeation *in vivo* still presents quite a challenge.

## **1.3 Iron, oxidative stress and neurodegeneration**

### **1.3.1 Iron**

Iron is essential for all living cells, playing a vital role in processes such as oxygen transport, electron transfer, DNA synthesis and enzymatic reactions. Nevertheless, if present in excess, iron can be toxic through the generation of free radicals. Iron homeostasis in the human body is thus strictly controlled on a cellular and systemic level (Camaschella and Strati, 2010; Liu and Hider, 2002).

In plasma, iron is bound to the glycoprotein transferrin and transferrin bound iron is transported into the cells via the transferrin receptor (Hentze et al., 2010). Iron delivery to the CNS takes place via the transferrin route or via non-transferrin-bound iron pathways involving divalent metal transporter 1 or lactoferrin and ferritin and their receptors (Li et al., 2010).

In neurons iron is stored in the lysosome or bound to sequestration proteins like ferritin or neuromelanin (Li et al., 2010) and iron homeostasis is controlled through

posttranscriptional regulation via the iron regulatory protein (IRP)/ iron responsive element (IRE) system (Gille and Reichmann, 2011). According to intracellular iron levels the IRP undergoes structural changes which result in a change of binding affinity for the IRE located in either the 3' or 5' untranslated region of the target protein's mRNA. The expression of proteins involved in iron uptake, storage, transport and utilization are therefore controlled by intracellular iron concentrations (Altamura and Muckenthaler, 2009). For example, iron depletion induces IRP binding in the 3' untranslated region of the transferrin receptor mRNA, which stabilizes it and increases translation subsequently promoting more iron to be transported into the cells. In contrast, iron repletion induces binding in the 5' untranslated region of transferrin receptor mRNA, which inhibits its translation (Li et al., 2010; Hentze et al., 2010).

In the brain iron is required for both neurodevelopment and normal function (Horowitz and Greenamyre, 2010), since iron is a cofactor in enzymes involved in the synthesis and metabolism of neurotransmitters as well as being involved in the process of axon myelination (Altamura and Muckenthaler, 2009; Horowitz and Greenamyre, 2010).

### **1.3.2 Oxidative stress**

Oxidative stress is characterized as an imbalance between the production of free radicals and the antioxidant defence system of the cell (Hider et al., 2011). A free radical is defined as a molecule or atom with an unpaired electron, rendering it unstable and reactive (Higgins et al., 2010; Jomova et al., 2010). Under physiological conditions free radicals are by-products of intracellular oxygen metabolism, being generated during the oxidative phosphorylation in mitochondria (Higgins et al, 2010). The most important are derived from oxygen (ROS, reactive oxygen species) including the superoxide ( $O_2^{\cdot-}$ ), hydroxyl ( $OH^{\cdot}$ ) and nitric oxide ( $NO^{\cdot}$ ) radical. However, the non-radicals hydrogen peroxide ( $H_2O_2$ ) and peroxynitrite ( $ONOO^{\cdot}$ ) also contribute to the cells redox state (Hider et al., 2011). As a defence against free radicals the body has various systems that include superoxide dismutase, catalase, glutathione and vitamin E (Higgins et al., 2010; Hider et al., 2011).

Iron is bound to sequestration proteins and safely liganded in enzymes considering that free or poorly liganded Fe(II) can participate in the Fenton reaction, which leads to the generation of the hydroxyl radical (Jamova et al., 2010; Kell, 2010).



**Scheme 1: Fenton reaction**

The hydroxyl radical, as well as other free radicals, is able to react with biomolecules such as DNA, RNA, lipids and proteins causing oxidative modifications in the molecules. These modified biomolecules can accumulate intracellularly, which can further lead to dysfunction and through the activation of various signalling pathways can result in cell death (Hider et al., 2011; Salvador et al., 2010).

### **1.3.3 Neurodegeneration and oxidative stress**

Neurodegenerative diseases involve the progressive death of neurons, usually affecting disease specific types of neurons (Gaeta and Hider, 2005). The primary risk factor for neurodegenerative diseases is age, which is linked to increased oxidative stress, and oxidative stress has been shown to play a key role in the pathology of various neurodegenerative diseases (Molina-Holgado et al., 2007). Common features are found in diseases such as Alzheimer's and Parkinson's disease, that include the aggregation of modified proteins, the accumulation of which is neurotoxic, high levels of metals and oxidative damage. The brain and its sensitive neurons are at particular risk of oxidative damage, since the brain accounts for about 20% of total body oxygen consumption. Additionally, relatively low levels of antioxidants are present and the brain has a tendency to accumulate metals with age, which might provide the link between oxidative stress and protein aggregation (Molina-Holgado et al., 2007).

#### **1.3.3.1 Alzheimer's disease**

Alzheimer's disease (AD) is the most common neurodegenerative disease, affecting about 18 million people worldwide and clinically manifests with cognitive impairment, memory loss and dementia (Kerche and Barnham, 2011). Its characteristic pathological hallmarks are the presence of intracellular neurofibrillary tangles consisting of the hyperphosphorylated microtubule-associated protein tau, and the extracellular deposition of senile plaques consisting of amyloid  $\beta$  ( $\text{A}\beta$ ) (Ballard et al., 2011).

Out of the different isoforms of  $\text{A}\beta$  (39-42 amino acids in length) that originate from proteolytic cleavage of the amyloid precursor protein APP,  $\text{A}\beta(1-42)$  is found to be particularly toxic to cells due to its fibrillogenic activity (Hider et al., 2011).  $\text{A}\beta(1-42)$

can bind Zn(II), Cu(II) and Fe(III) via 3 histidine and a methionine residue in the peptide (Altamura and Muckenthaler, 2009; Molina-Holgado et al., 2007), thus mediating the formation of free radicals as a consequence of metal binding (Tabner et al., 2005; Hider et al., 2011). Iron is found to accumulate in the same regions as A $\beta$  extracellularly and intracellularly in neurons containing neurofibrillary tangles (Salvador et al., 2010; Horowitz and Greenamyre, 2010). Iron concentrations in the brain are 3-5 times higher when compared to age matched controls (Molina-Holgado et al., 2007) and both A $\beta$  aggregation and tau hyperphosphorylation have been shown to be inducible by iron (Horowitz and Greenamyre, 2010). Additionally, A $\beta$  is reported to participate in a vicious cycle, where oxidative stress induces A $\beta$  production, and the oxidative stress associated with metal binding and A $\beta$  aggregation in turn enhances A $\beta$  production yet again (Molina-Holgado et al., 2007; Salvador et al., 2010).

### **1.3.3.2 Parkinson's disease**

Parkinson's disease (PD) is characterized by the selective degeneration of dopaminergic neurons in the substantia nigra pars compacta, which leads to a significant loss of dopamine in the striatum, causing symptoms like tremor, bradykinesia, dyskinesia and rigidity (Schapira et al., 2006; Altamura and Muckenthaler, 2009). Additionally, intracellular inclusions of protein aggregates (Lewy Bodies) are found, which mainly consist of  $\alpha$ -synuclein. Iron tends to accumulate in the Lewy Bodies, where it has been shown to be able to promote and induce  $\alpha$ -synuclein aggregation (Altamura and Muckenthaler, 2009; Snyder and Connor, 2010). Through the interaction with  $\alpha$ -synuclein iron can mediate the generation of free radicals causing oxidative damage as a consequence. Oxidative damage is found in PD post-mortem brains affecting DNA, lipids and proteins (Hider et al., 2011).

Furthermore, ferritin levels in the PD brain are lower and ferritin is highly loaded with iron compared to controls (Altamura and Muckenthaler, 2009). As a consequence of increased iron levels, neuromelanin is oversaturated with iron, thus the loosely bound iron retains its redox activity and can generate the formation of free radicals (Horowitz and Greenamyre, 2010; Gaeta and Hider, 2005). Moreover, mitochondria dysfunction and reduced levels of antioxidants like glutathione are also found in PD post-mortem brains (Molina-Holgado et al., 2007).

### 1.3.3.3 Friedreich's Ataxia

Friedreich's Ataxia is an autosomal recessive degenerative disease that involves the expansion of a trinucleotide repeat in the first intron of the gene encoding for the mitochondrial iron chaperone protein fraxitin (Boddaert et al., 2007). This leads to a decreased expression of fraxitin and therefore an increase in mitochondrial iron levels. Subsequently, the high iron levels result in iron-mediated oxidative damage affecting the sensory neurons, the heart and the endocrine glands (Whitnall and Richardson, 2006).

### 1.3.4 Iron chelation as a therapeutic strategy

It is still a matter of scientific debate whether oxidative stress associated with high levels of metals like copper, zinc and iron in the brain is the primary cause or a result of the progression of neurodegenerative diseases like AD and PD. Nevertheless, it provides a promising new target for the treatment of these diseases (Gaeta and Hider, 2005).

There are several factors that need to be taken into consideration when designing a clinical useful chelator. First of all, metal selectivity is a key factor, especially in reducing side effects of chelation therapy. In the case of AD, copper, iron and zinc have been shown to contribute to the disease, whereas in PD iron is the main identified metal involved (Hider et al., 2011).

Iron chelators can be structurally classified according to the number of donor atoms interacting with the iron ion. When six donor atoms are present in one single molecule, it is referred to as hexadentate, when 2, 3 or more coordinating donor atoms are present in one molecule, the chelator is named bidentate, tridentate or multidentate respectively (Liu and Hider, 2002).

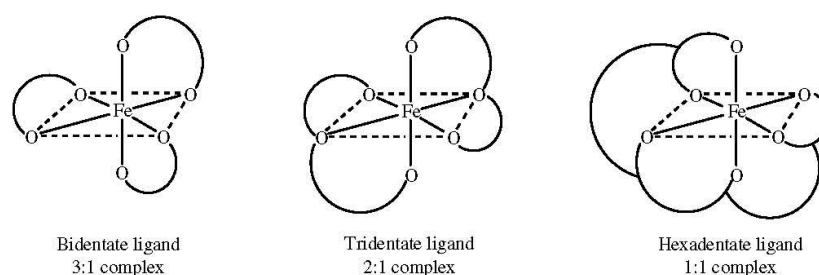


**Figure 4: Schematic representation of iron-ligand complexes (from Gaeta and Hider, 2005)**

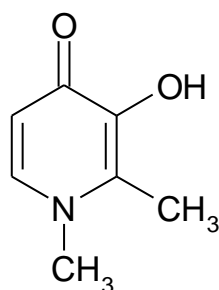
Chelators can be designed to be selective for either Fe(II) or Fe(III). Selective Fe(II) chelators use nitrogen atoms as donor atoms, whereas Fe(III) selective chelators use oxygen atoms. There are major advantages for the use of Fe(III) selective chelators, since Fe(II) chelators also have an affinity to bind bivalent metals such as Cu(II) and Zn(II). Contrary to copper and zinc, tribasic metals like aluminium(III) and gallium(III) are not essential for living cells, rendering Fe(III) selective chelators the therapeutic strategy for iron chelation (Hider et al., 2008). Furthermore, Fe(III) selective chelators can also bind Fe(II) under aerobic conditions and induce autoxidation to Fe(III), which enables them to bind iron under most physiological conditions (Hider et al., 2008).

For the successful application of iron chelators in the treatment of neurodegenerative diseases, it is necessary for the chelator to be able to scavenge the redox active iron from the brain. Additionally beneficial would be the ability to scavenge the labile iron from its binding site as well to prevent mediated oxidative damage (Hider et al., 2008). Preferably a non-charged complex of the chelator with iron should be formed to facilitate efflux through passive diffusion, thereby removing the iron from the brain (Hider et al., 2011). To achieve this, a chelator must first of all have the ability to cross the blood-brain barrier (BBB). Therefore it is suggested that the size is limited to less than 400 Da, which eliminates hexadentate chelators from consideration. Lipophilic drugs tend to be able to cross the BBB better than hydrophilic drugs, but liver first pass effect as a consequence of increased lipophilicity of the chelator must not be neglected (Hider et al., 2011).

A problem associated with iron chelation therapy is toxicity due to inhibition of iron containing enzymes. Iron chelators have been shown not to directly inhibit haem containing enzymes since the porphyrin bound iron is inaccessible, nevertheless non-haem containing enzymes such as lipoxygenase, the aromatic hydroxylase family and ribonucleotide reductase can be affected (Hider et al., 2011). For the potential application of iron chelators for the treatment of neurodegenerative diseases, possible interactions with the enzymes involved in the synthesis and metabolism of dopamine and serotonin have to be taken into careful consideration as well. By modifying the physicochemical properties of the chelating agent it is possible to limit such interactions (Hider et al., 2011).

### 1.3.4.1 Hydroxypyridinones

Hydroxypyridinones (HPO) are bidentate iron chelators that form a stable and non-charged 3:1 complex with Fe(III). Out of this class, 3-hydroxypyridin-4-ones have the highest affinity for Fe(III) (Liu and Hider, 2002) and the complexes with Fe(III) have an extremely low redox potential (Hider et al., 2011). The most prominent 3-hydroxypyridin-4-one is deferiprone (Ferriprox<sup>®</sup>), which is the only orally active iron chelator available. Deferiprone is successfully used for the treatment of iron overload associated with the genetic haematological disease  $\beta$ -Thalassaemia (Liu and Hider, 2002). Due to the fact that deferiprone forms neutral complexes with iron and its small size, it is able to permeate membranes by passive diffusion and eliminate iron from various tissues including the heart (Hider et al., 2011).



**Formula 1: deferiprone**

Moreover, its ability to cross the BBB has been shown and deferiprone has been introduced as a treatment for patients suffering from Friedreich's Ataxia (Hider et al., 2011). In addition, the application of deferiprone in other neurodegenerative diseases associated with iron-mediated oxidative stress like Alzheimer's and Parkinson's disease has been suggested and deferiprone is currently under investigation in a clinical trial for the treatment of Parkinson's disease.

Even though deferiprone has a moderate ability to cross the BBB, the search for more efficient chelators continues. Therefore a series of fluorinated 3-hydroxypyridin-4-ones has been designed and synthesized to enhance BBB permeability without increasing liver first pass effect (Ma and Hider, 2010; Hider et al., 2011). Some of these compounds have been used in the following study.

## 1.4 Aims and objectives

Primary porcine brain endothelial cells (PBEC) were used as an *in vitro* model to assess the blood-brain barrier permeability of six 3-hydroxypyridin-4ones (HPO). For the selected HPOs, *in vivo* data was already available. Thus, the aim was to investigate whether it is possible to correlate *in vivo* and *in vitro* data, which would allow predictions of *in vivo* blood-brain barrier permeability to be made from *in vitro* data.

The objectives were defined as follows:

- assessing toxicity of the 3-hydroxypyridin-4ones on PBECs
- assessing the effect of different culture conditions on the quality of the PBEC monolayer
- assessing blood-brain barrier permeability of the 3-hydroxypyridin-4ones *in vitro*
- correlating *in vivo* and *in vitro* data



## **2 MATERIALS AND METHODS**

### **2.1 Materials**

#### **2.1.1 Chemicals**

All chemicals were obtained from Sigma Aldrich unless stated otherwise. Bovine plasma derived serum (BPDS) was purchased from FirstLink UK, RO-20-1724 was purchased from Calbiochem and Dulbecco's modified eagle medium (DMEM) was obtained from Invitrogen. The Thermo Scientific Pierce BCA Protein Assay Kit was purchased from Thermo Scientific. Acetonitrile (HPLC gradient grade) and 1-heptane sulfonic acid were obtained from Fisher Scientific UK. The 3-hydroxypyridin-4ones (HPOs) used in this study were synthesized by Dr. Yong Min Ma. Structures and physicochemical properties are shown in Table 1.

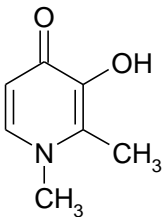
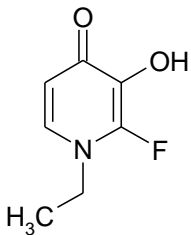
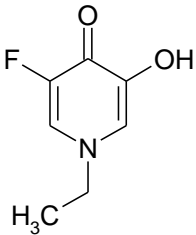
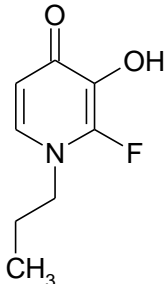
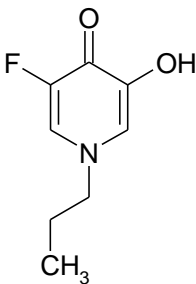
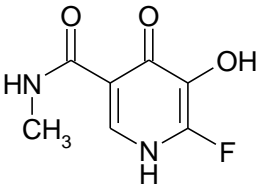
#### **2.1.2 Cells**

Primary porcine brain endothelial cells (PBEC) were obtained from Ana Georgian and Siti Yusof using the isolation protocol described in 2.2.1.1. Primary astrocytes were obtained from Siti Yusof and C6 glioblastoma were received as gift to the King's College London Blood-Brain Barrier group from the Babraham Institute, Cambridge.

#### **2.1.3 Analytical apparatus**

A Labsystems Multiskan Ascent microplate reader was used to measure absorbance for the MTT and BCA assay. To measure fluorescence for the analysis of sodium fluorescein concentrations, a FlexStation microplate reader was used. Transendothelial electrical resistance (TEER) was measured using an STX100 probe and an EVOM volt-ohmmeter. HPLC was performed on a Waters system consisting of a 717plus Autosampler, a 2996 Photodiode Array Detector, a 600s Controller and a 626 Pump.

**Table 1: Structure, molecular weight (MW) and  $\log D_{7.4}$  of the HPOs used in this study**

Compound	Structure	MW	$\log D_{7.4}$
CP20		139	-0.77
YMF 8		157	-0.75
YMF 16		157	-0.95
YMF 24		171	-0.05
YMF 25		171	-0.54
YMF 29		186	-1.00

## 2.2 Methods

### 2.2.1 Cell culture

#### 2.2.1.1 Cerebral microvessel endothelial cell isolation

Porcine brain endothelial cells (PBEC) were isolated based on the methods of Rubin et al. (1991), and Skinner et al. (2009). Porcine brains were obtained from a slaughterhouse and transported in L-15 medium containing  $100\text{U.mL}^{-1}$  penicillin and  $100\mu\text{g.mL}^{-1}$  streptomycin. The brain hemispheres were washed in phosphate-buffered saline (PBS), cleared of meninges and stored in ice cold PBS. After the removal of the white matter, the brain tissue was sliced into small pieces and homogenized in MEM/HEPES media containing 10% (v/v) fetal calf serum (FCS). Subsequently the homogenate was filtered through a  $150\mu\text{m}$  nylon mesh, followed by filtration through a  $60\mu\text{m}$  nylon mesh. The brain tissue on both meshes was then digested using M199 medium containing 10% (v/v) FCS,  $100\text{U.mL}^{-1}$  penicillin,  $100\mu\text{g.mL}^{-1}$  streptomycin,  $210\text{ U.mL}^{-1}$  collagenase,  $114\text{ U.mL}^{-1}$  DNase I and  $91\text{ U.mL}^{-1}$  trypsin-EDTA for 1 hour at  $37^\circ\text{C}$ . The digestive mix was washed off the mesh with MEM/HEPES and centrifuged for 10 minutes at  $1000 \times g$ . The pellet, formed by the cerebral microvessels, was then resuspended in FCS containing 10% (v/v) DMSO. One mL aliquots were frozen at  $-80^\circ\text{C}$  for 24h and then moved into liquid nitrogen, where the cerebral microvessels were stored for further use. Isolations were performed by Ana Georgian and Siti Yusof.

#### 2.2.1.2 Defrosting PBECs

Two T-75 flasks were each coated with 4ml of rat tail collagen ( $100\mu\text{g.mL}^{-1}$ ), at room temperature, for a minimum of 2 hours. The flasks were washed twice with 4mL HBSS and then coated with 4mL fibronectin ( $7.5\mu\text{g.mL}^{-1}$ ) each, at room temperature, for a minimum of 2 hours. The coating was removed and the flasks were washed twice with 4ml HBSS each. Afterwards, PBEC media (DMEM containing 10% (v/v) BPDS,  $100\text{U.mL}^{-1}$  penicillin,  $100\mu\text{g.mL}^{-1}$  streptomycin, 2mM L-glutamine and  $125\mu\text{g.mL}^{-1}$  heparin) was prepared and  $4\mu\text{g.mL}^{-1}$  puromycin was added to the PBEC media before sterile filtration (pore size  $0.2\mu\text{m}$ ).

Puromycin is a P-gp substrate used to purify endothelial cell cultures. Since endothelial cells highly express P-gp, puromycin is actively effluxed out of the endothelial cells, hence concentrations otherwise toxic can be used. In contrast to endothelial cells,

contaminating cell types (for example fibroblasts or pericytes) lack P-gp expression and will not survive the puromycin treatment (Perrière et al. 2005).

The freshly prepared PBEC media was warmed in a water bath and then used to resuspend PBECs that were stored in liquid nitrogen. Subsequently, 10mL of cell suspension was placed into each of the pre-coated flasks. PBECs were kept in an incubator at 37°C and 5% CO<sub>2</sub>. The media was replaced with freshly prepared media without puromycin after 3 days.

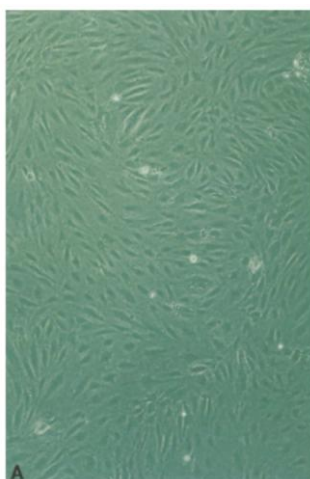


**Figure 5: Confluent PBEC monolayer (from Bobilya et al., 1995)**

### 2.2.1.3 Passaging PBECs

PBECs were passaged when growth reached 30% confluence and small clusters of cells were visible which was closely monitored using an inverted light microscope. PBECs reached that state after 3-6 days in culture.

For passaging, each T-75 flask of cells was washed twice with 10mL HBSS (with phenolred, without Ca<sup>2+</sup> and Mg<sup>2+</sup>) before 2.5mL of trypsin-EDTA was added and the flasks were placed into the incubator at 37°C. After 8-10min in the incubator, the number of cells that had detached from the bottom of the flask was determined using the inverted light microscope, while gently tapping the flask. If necessary, the flasks were placed into the incubator at 37°C for further 5min. When 80% of the cells had detached from the bottom of the flask, 8mL of freshly prepared warm PBEC media was added to each flask and the cells were pooled into a universal tube for centrifugation. After PBECs were centrifuged at 1500 rpm for 5 min, the supernatant was removed and the cell pellet was

resuspended in 1mL PBEC media (DMEM containing 10% (v/v) BPDS, 100U.mL<sup>-1</sup> penicillin, 100µg.mL<sup>-1</sup> streptomycin, 2mM L-glutamine and 125µg.mL<sup>-1</sup> heparine).

From the cell suspension 10µL was removed to count cells using a haemocytometer. PBECs were then resuspended in the correct amount of media and seeded into either a 96 well plate or into the Transwell® system.

For seeding PBECs into a 96 well plate, the plate was pre-coated with 200µL of rat tail collagen (100µg.mL<sup>-1</sup>) per well using the protocol described for coating culture flasks. PBECs were seeded at a density of  $0.3 \times 10^5$  cells per well.

For seeding PBECs into Transwell® filter inserts (polycarbonate filters, pore size 0.4µm, area 1.12cm<sup>2</sup>), Transwell® inserts were pre-coated with 500µL of rat tail collagen (100µg.mL<sup>-1</sup>) followed by 500µL of fibronectin (7.5µg.mL<sup>-1</sup>) as described for coating culture flasks. PBECs were seeded at a density of  $1 \times 10^5$  cells per filter insert.

For non-contact co-culture with C6 glioblastoma, PBECs were seeded into Transwell® inserts, which were placed above confluent C6 glioblastoma.

#### **2.2.1.4 Primary astrocytes**

Primary astrocytes were defrosted similarly to the PBECs. Two T-75 flasks were pre-coated with 4mL poly L-lysine (10µg.mL<sup>-1</sup>) each, for 30min at 37°C. Poly L-lysine coating was then removed and the flasks were left to dry at room temperature. Primary astrocytes, that were stored in liquid nitrogen, were resuspended in 10mL astrocyte media (DMEM (with high glucose and pyruvate) containing 10% (v/v) FCS and 100U.mL<sup>-1</sup> penicillin) before being placed into the pre-coated, dry flasks. Astrocytes were kept in an incubator at 37°C and 5% CO<sub>2</sub>.

##### **2.2.1.4.1 Collection of astrocyte-conditioned media**

Astrocytes grew confluent after 7-10 days in culture. When confluence was reached, the conditioned media was taken off every 2 days and replaced with freshly prepared astrocyte media. Astrocyte-conditioned media (ACM) was collected from primary astrocytes of up to 30 days in culture and conditioned media was either used immediately or stored at -20°C for further use.

### **2.2.1.5 C6 glioblastoma**

C6 glioblastoma cells (passage 130) were defrosted as described for the primary astrocytes, but without any pre-coating of the culture flasks. C6 glioblastoma were passaged into 12 well plates as described for PBECs using trypsin-EDTA and astrocyte media (DMEM (with high glucose and pyruvate) containing 10% (v/v) FCS and 100U.mL<sup>-1</sup> penicillin). C6 glioblastoma cells were seeded at a density of 1x10<sup>5</sup> per well and grew confluent within 3 days in culture (37°C and 5% CO<sub>2</sub>).

## **2.2.2 Assessing cell viability**

### **2.2.2.1 Cytotoxicity assay**

To assess the cytotoxicity of the HPOs on cultured PBECs, the MTT assay was used. This is a quantitative, calorimetric assay to determine cell viability. The quantification is based on the reduction of the tetrazolium salt MTT (3-(4,5-dimethylthiazol-2-yl)-2,5-diphenyl tetrazolium bromide) to a blue water insoluble formazan salt by the mitochondrial enzyme succinate dehydrogenase in living cells. The blue formazan salt can be dissolved in an organic solvent and the absorbance measured is directly proportional to the amount of living cells in the sample (Mosmann, 1983; Denizot and Lang, 1986).

The MTT assay was conducted in 96 well plates on 100% confluent PBECs. Solutions of 800µM HPO in assay buffer (HBSS, 25mM HEPES, 0.1% (v/v) BSA, pH 7.4) were prepared and warmed at 37°C. The media was removed from the PBECs and the cells were incubated with 200µL of the HPO-solutions per well for 2 hours at 37°C. HPO-solutions were removed and cells were washed twice with HBSS (200µL per well). Then, 100µL MTT-solution (1mg.mL<sup>-1</sup> MTT in DMEM (without phenolred)) was added to each well and incubated at 37°C and 5% CO<sub>2</sub> for 4 hours. To remove the well contents the plate was turned over and blotted, leaving just the blue crystals (formazan salt) that were formed on the bottom of the wells. The crystals were dissolved in 100µL propan-2-ol and absorbance at 540nm was measured on a Labsystems Multiskan Ascent microplate reader.

### **2.2.2.2 BCA protein assay**

The BCA Protein Assay is a quantitative colorimetric assay to determine the protein concentration of a sample based on the reduction of Cu<sup>2+</sup> to Cu<sup>1+</sup> by peptides in an alkaline medium. The Cu<sup>1+</sup> ion interacts with 2-bicinchoninic acid (BCA), forming a

purple water soluble complex with a measurable absorbance at 562nm. The absorbance measured correlates with the protein concentration in the sample. To calculate protein concentrations, a standard curve of bovine serum albumin (BSA) in known concentrations is used (Smith et al., 1985).

The BCA protein assay was conducted in 96 well plates on 100% confluent PBECs. HPO-solutions in assay buffer (HBSS, 25mM HEPES, 0.1% (v/v) BSA, pH 7.4) were prepared at a concentration of 800 $\mu$ M and warmed at 37°C. After the removal of the media, the PBECs were incubated with 200 $\mu$ L of the HPO-solution per well for 2 hours at 37°C. The solutions were then removed and 200 $\mu$ L Triton X (1% (v/v) in distilled water) was added to each well to lyse the cells for 45 minutes at 37°C. An aliquot of 100 $\mu$ L cell lysate was transferred to a new 96 well plate and incubated with 100 $\mu$ L BCA working reagent (solution A containing sodium carbonate, sodium bicarbonate, bicinchoninic acid and sodium tatrare in 0.2N sodium hydroxide and solution B containing 4% cupric sulphate; A:B = 50:1) for 30 minutes at 37°C. Standards of 100 $\mu$ L BSA in different concentrations (0, 10, 15, 20, 25 and 30 $\mu$ g.mL<sup>-1</sup>) were incubated with the BCA working reagent alongside the samples as described above. The absorbance at 562nm was measured using a Labsystems Multiskan Ascent microplate reader and protein concentrations were calculated using the BSA standard curve produced by Ascent Software.

### **2.2.2.3 Calculating overall cell viability**

To get a correct value for cell viability, the MTT assay was conducted on half the wells, for the other half a BCA assay was done. Overall cell viability was calculated and expressed as absorbance measured per  $\mu$ g protein. PBECs not treated with HPO served as a control to evaluate the results.

### **2.2.3 Permeability assay**

To study the transport of the HPOs across the blood-brain barrier *in vitro*, a Transwell® system was used. PBECs were grown in Transwell® inserts with polycarbonate filters (pore size 0.4 $\mu$ m; area 1.12cm<sup>2</sup>) suspended above 12 well plates. In this experimental set up, the donor chamber (apical chamber) mimics the apical side of the endothelium (blood) whereas the receiver chamber (basolateral chamber) mimics the basolateral side of the endothelium (brain) as shown in Figure 6.

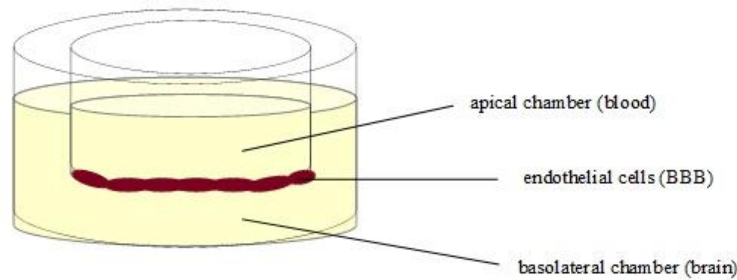


**Figure 6: Schematic representation of a Transwell® insert used for the *in vitro* permeability assay**

### 2.2.3.1 Culture conditions

PBECs in Transwell® inserts were grown under 3 different culture conditions.

- PBECs grown in monoculture
- PBECs grown in monoculture and treated with 50% astrocyte-conditioned media (ACM) on the basolateral chamber
- PBECs grown in non-contact co-culture with C6 glioblastoma cells, with C6 glioblastoma grown on the bottom of the 12 well plates underneath the filter insert (Figure 7)

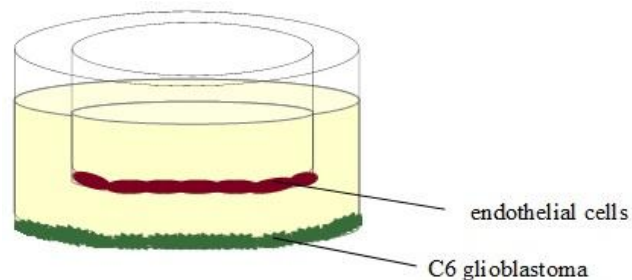


**Figure 7: Schematic representation of a Transwell® insert with PBECs grown in non-contact co-culture with C6 glioblastoma**

### 2.2.3.2 Enhancing barrier properties

PBECs were passaged into Transwell® inserts and grew confluent within 3 days. Since polycarbonate filters are opaque, PBECs seeded on polyethylene filter inserts (see-through) served as a reference to monitor the growth. After confluence was reached, the media was replaced with serum free PBEC media (DMEM,  $100\text{U}\cdot\text{mL}^{-1}$  penicillin,



100 $\mu\text{g.mL}^{-1}$  streptomycin, 2mmol.L $^{-1}$  L-glutamine and 125 $\mu\text{g.mL}^{-1}$  heparin) that was additionally supplemented with 550nM hydrocortisone. Furthermore, PBECs were treated with 250 $\mu\text{M}$  8-4-chlorophenylthio-cAMP (CTP-cAMP) and 17.5 $\mu\text{M}$  of phosphodiesterase inhibitor RO-20-1724 (RO).

#### 2.2.3.2.1 Treatment for the different culture conditions

PBECs in monoculture and PBECs grown in non-contact co-culture with C6 glioblastoma received treatment with serum free media, hydrocortisone, CPT-cAMP and RO.

PBECs grown with astrocyte-conditioned media (ACM) were treated with serum free media, hydrocortisone, CPT-cAMP and RO as described above. Additionally, ACM was supplemented into the basolateral chamber at a concentration of 50% using the ACM harvested from primary astrocytes.

### 2.2.3.3 Determining the quality of the barrier

#### 2.2.3.3.1 Measurement of TEER

After 24 hours of treatment with serum free media, hydrocortisone, CPT-cAMP and RO, transendothelial electrical resistance (TEER) was measured using an STX100 probe and an EVOM volt-ohmmeter.

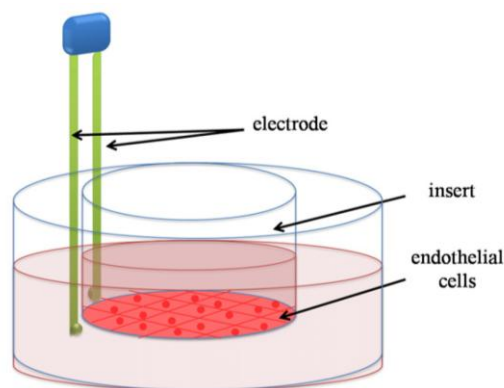
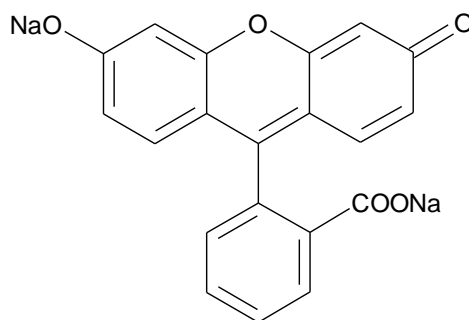


**Figure 8: Schematic representation of the TEER measurement with copstick electrodes (from Cardoso et al., 2010)**

TEER represents the movement of small ions via the paracellular pathway and depends on the amount and complexity of tight junctions formed between the endothelial cells. Therefore TEER measurements were carried out before the permeability assay to determine the quality of the barrier.

Final electrical resistance of the PBEC monolayer was calculated by subtracting the value of a collagen coated Transwell® insert (no cells) from the resistance measured for the insert with PBECs and multiplied by the area of the Transwell® insert. TEER is expressed in  $\Omega \cdot \text{cm}^2$ .



**Formula 2: sodium fluorescein**

#### 2.2.3.3.2 Paracellular marker

To further assess the quality of the endothelial cell barrier, sodium fluorescein was used as a paracellular marker during the permeability assay. Sodium fluorescein is known not to penetrate into endothelial cells, so when added to the apical chamber its only route of transfer to the basolateral chamber is via the paracellular route. Therefore, measuring the permeability of sodium fluorescein to the basolateral chamber is indicative of the tightness of the junctions formed between the PBECs.

#### 2.2.3.4 Experiment protocol

The wells of 12 well plates were filled with 1.5mL assay buffer (HBSS, 25mM HEPES, 0.1% (v/v) BSA, pH 7.4) and warmed to 37°C. Solutions of 800 $\mu\text{M}$  HPO in permeability buffer (assay buffer containing sodium fluorescein (10 $\mu\text{g} \cdot \text{mL}^{-1}$ )) were prepared and also warmed at 37°C. The media was removed from both apical and basolateral chamber of the PBEC cultures and the Transwell® inserts were placed into the 12 well plates that already contained the 1.5mL of warm assay buffer (basolateral chamber). To the apical chamber of the inserts, 500 $\mu\text{L}$  HPO-solution in permeability buffer was added and the plates were shaken at 200 rpm in an orbital shaker at 37°C. After 20 minutes, the inserts were moved into a new 12 well plate to prevent any transport into the basolateral chamber while samples were taken from both the apical and the basolateral chamber.

To determine the concentration of the paracellular marker sodium fluorescein, 100 $\mu\text{L}$

samples were taken from the apical and basolateral chamber and pipetted into a 96 well plate. The 96 well plate also contained assay buffer (0% sodium fluorescein) and permeability buffer in different concentrations (100%, 90%, 75%, 25%, 12.5%, 6.25%, 3.125%, 1.56%, 0.78%, 0.39% sodium fluorescein) to establish a standard curve. Fluorescence was measured at an excitation wavelength of 485nm and an emission wavelength of 530nm, and sodium fluorescein concentrations in the samples were calculated according to the standard curve.

To determine the concentration of HPO transferred through the cell monolayer, 300 $\mu$ L samples were taken from the apical chamber and 1.3mL samples were taken from the basolateral chamber for further analysis with HPLC.

#### **2.2.3.5 Correcting HPO transfer**

HPO concentrations in the basolateral chamber were determined at the end of the permeability assay and then corrected for paracellular transfer. Thus, data acquired for sodium fluorescein transfer was used to determine the proportion of HPO transfer via the paracellular route and subtracted from the overall HPO transfer.

#### **2.2.3.6 Calculating intracellular accumulation**

Intracellular accumulation was defined and calculated as the HPO concentration not recovered after summing the concentrations determined for both apical and basolateral chamber at the end of the permeability assay, compared to the initial HPO concentration in the apical chamber.

### **2.2.4 HPLC**

To determine HPO concentrations in the samples taken from the permeability assay, high performance liquid chromatography (HPLC) was used.

HPLC was performed using a reversed-phase polymer column (PLRP-S 300 $\text{\AA}$ , 15 x 0.46 cm, internal diameter 8 $\mu$ m). A gradient ion-pair method (Liu et al., 1999) was applied, using 5mM 1-heptanesulfonic acid sodium salt (adjusted to pH 2 using HCl) as the ion-pair buffer. A gradient of 2-35% acetonitrile over 20 minutes was followed by a post-run of 5 minutes to restore initial conditions (2% acetonitrile and 98% buffer). The flow rate was 1mL/min and HPOs were monitored at 280nm. 100 $\mu$ L of the samples were injected as quadruples.

Standard curves of all HPOs were produced prior to the permeability assay, using different concentrations of the HPOs (1000, 750, 500, 200, 100, 50, 25, 10, 5 $\mu$ M) in HPLC-water. Injections of 100 $\mu$ L were done in quadruples and the area under the curve (AUC) was plotted against the concentration to establish a standard curve. These standard curves were used to calculate the concentration of the HPOs in the samples from the permeability assay.

Chromatograms were produced and analysed by Millennium Software.

### **2.2.5 Statistical analysis**

Statistical analysis of the experimental data was conducted with Graph Prism 5 using one way ANOVA and Tukey's multiple comparison test as the post test.

### 3 RESULTS

#### 3.1 Viability

In order to accurately compare the *in vitro* and *in vivo* data, the concentration used to perform the *in vivo* experiments (800 $\mu$ M) was aimed to be used in the *in vitro* assays as well. Hence, it was investigated whether this concentration affected PBEC viability before the permeability assays were performed. The viability was assessed using the MTT and the BCA assay.

##### 3.1.1 CP20

Since CP20 (deferiprone) served as the reference HPO in this study, its effect on PBECs was investigated first. PBECs were exposed to CP20 for 2 hours at a concentration of 100 $\mu$ M, 400 $\mu$ M and 800 $\mu$ M. PBECs not exposed to CP20 were used as a control to evaluate the results.

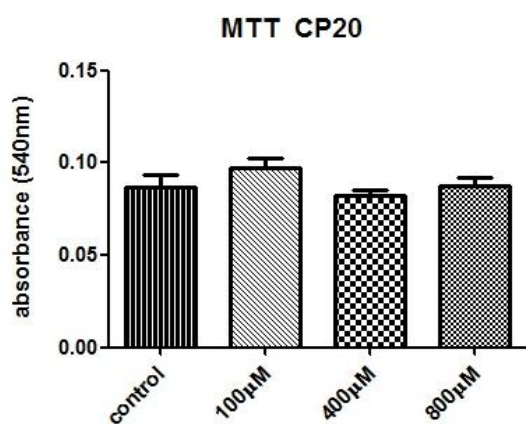


Figure 10: Absorbance measured at 540nm, after the MTT assay was conducted on PBECs incubated with CP20 for 2 hours.

Data is represented as mean  $\pm$  SEM (n=4).

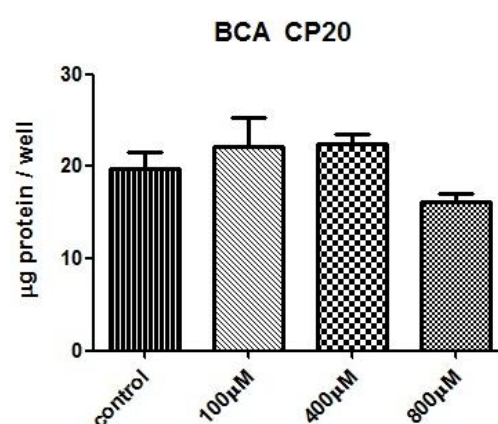
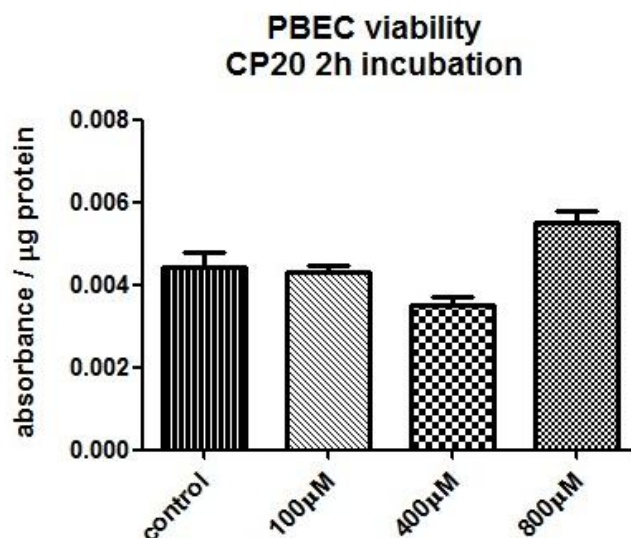


Figure 9: Protein content per well in  $\mu$ g, determined after performing the BCA assay on PBECs incubated with CP20 for 2 hours.

Data is represented as mean  $\pm$  SEM (n=4).



**Figure 11: PBEC overall viability after incubation with CP20 for 2 hours, expressed in absorbance per  $\mu\text{g protein}$ . Data is represented as mean  $\pm$  SEM (n=4).**

Overall viability was calculated using data from the MTT and the BCA assay as described in methods and materials (2.2.2.3) and expressed as absorbance measured per  $\mu\text{g protein}$ .

No statistically significant difference was found between the viability of PBECs in the control group compared to PBECs that were exposed to 100 $\mu\text{M}$  and 400 $\mu\text{M}$  CP20 after the 2 hour incubation. Furthermore, PBECs remained viable after 2 hour incubation with 800 $\mu\text{M}$  CP20 compared to control (Figure 11).

### **3.1.2 HPO viability**

CP20 could be shown not to be toxic to PBECs at the concentration of 800 $\mu\text{M}$  over 2 hours, hence the effect of the other HPOs on PBEC viability was assessed using the same concentration. The permeability assays were planned to be performed for 20min, therefore PBECs were incubated with 800 $\mu\text{M}$  of HPO solution for 20min. The effect of the exposure to 800 $\mu\text{M}$  HPO solution for 2 hours was determined as well.

### 3.1.2.1 Viability after 20min incubation

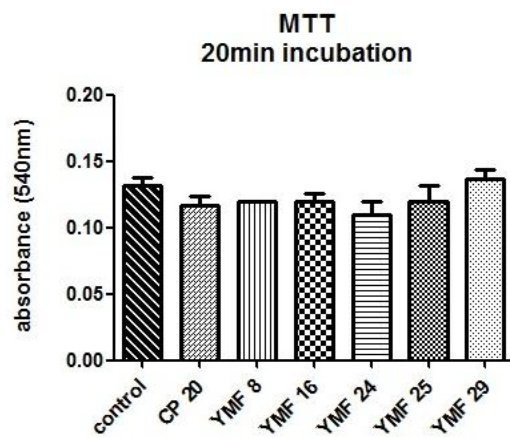


Figure 13: Absorbance measured at 540nm, after the MTT assay was conducted on PBECS incubated with 800µM HPO for 20min. Data is represented as mean  $\pm$  SEM (n=3).

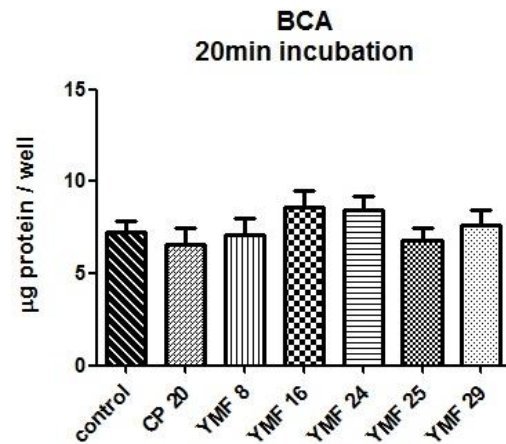


Figure 12: Protein content per well in µg, determined after performing the BCA assay on PBECS incubated with 800µM HPO for 20min. Data is represented as mean  $\pm$  SEM (n=3).

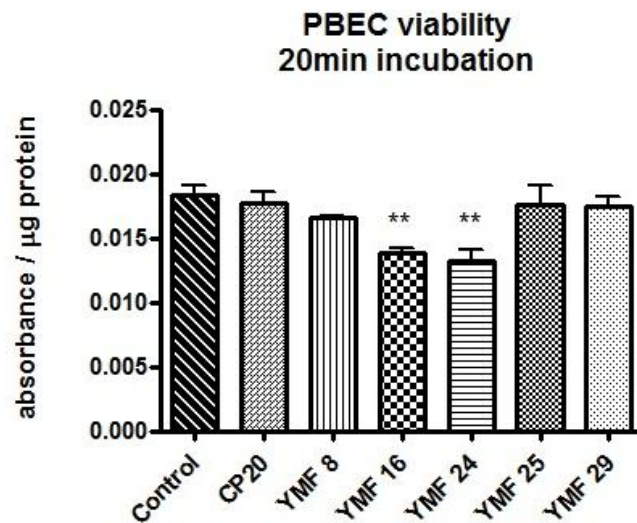


Figure 14: PBEC overall viability, expressed in absorbance per µg protein, after incubation with 800µM HPO for 20min.

Data is represented as mean  $\pm$  SEM (n=3).

Difference from control: \*\* p < 0.01

Only compounds YMF 16 and YMF 24 reduced PBEC viability after 20min exposure to 800 $\mu$ M (Figure 14) with  $75 \pm 2.58\%$  of PBECs remaining viable after incubation with YMF 16 and  $71.61 \pm 4.86\%$  in the case of PBECs incubated with YMF 24, compared to control. For compound YMF 8, YMF 25 and YMF 29 no toxic effect on the PBECs was found after 20min incubation.

### 3.1.2.2 Viability after 2 hour incubation

Following the assessment of PBEC viability for an incubation time of 20min with 800 $\mu$ M HPO solution, the effect of a longer exposure was studied using 2 hours as the end time point.

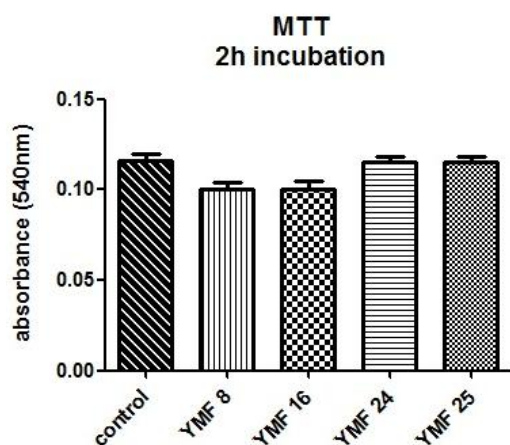


Figure 15: Absorbance measured at 540nm, after the MTT assay was conducted on PBECs incubated with 800 $\mu$ M HPO for 2 hours. Data is represented as mean  $\pm$  SEM (n=3).

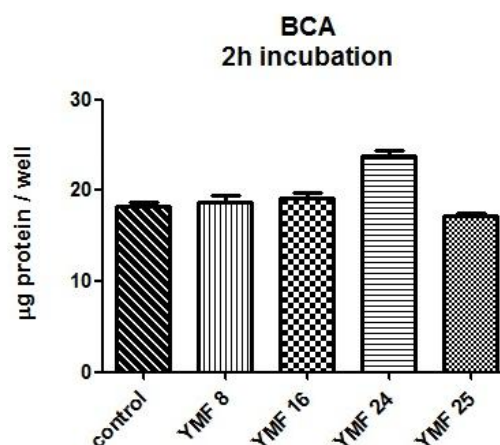
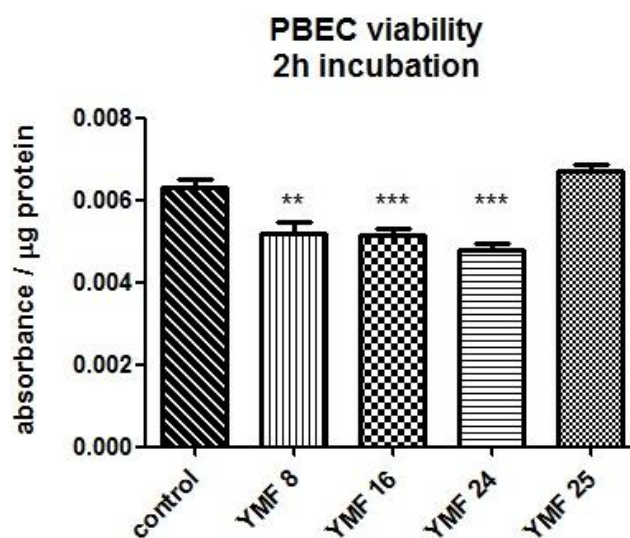


Figure 16: Protein content per well in  $\mu$ g, determined after performing the BCA assay on PBECs incubated with 800 $\mu$ M HPO for 2 hours. Data is represented as mean  $\pm$  SEM (n=3).





**Figure 17: Overall viability, expressed in absorbance per µg protein for PBECs incubated with 800µM HPO for 2 hours.**

**Data is represented as mean ± SEM (n=3).**

**Difference from control: \*\* p< 0.01/ \*\*\* p< 0.001**

After a 2 hour exposure of PBECs to 800µM HPO solution, compound YMF 16 and YMF 24 reduced viability as has been observed after incubation for 20min. Moreover, after the exposure time of 2 hours also compound YMF 8 showed an effect on the viability of the PBECs, whereas it had not been found to affect viability after 20min. However,  $82.79 \pm 3.89\%$  of PBECs treated with YMF 8 remained viable when compared to control cells. In the case of PBECs incubated with compounds YMF 16 and YMF 24, compared to control,  $81.14 \pm 2.79\%$  and  $76.31 \pm 2.20\%$  of cells remained viable respectively. Compound YMF 25 had no toxic effect on PBECs even after 2 hours of exposure.

### 3.2 CP20 time-dependent transport

The time-dependent transport across the PBEC monolayer was determined for CP20, the reference HPO in this study. In the *in vivo* experiments 20min was used as the end time point for the *in situ* brain perfusion. Hence it was necessary to evaluate whether CP20 transport during the 20min *in vitro* assay was sufficient in order to enable quantitative analysis with HPLC.

Therefore, Transwell® inserts were moved to a new basolateral chamber filled with assay buffer at different time points and CP20 concentrations were determined for each of these time points.

Three different experimental conditions were applied. For condition 1 Transwell® inserts were moved at 5, 10, 20, 30, 40 and 60min. For condition 2 the Transwell® inserts were moved only at 20, 40 and 60min. Condition 3 involved no Transwell® insert moving and CP20 concentrations were only determined at the last time point of 60min.

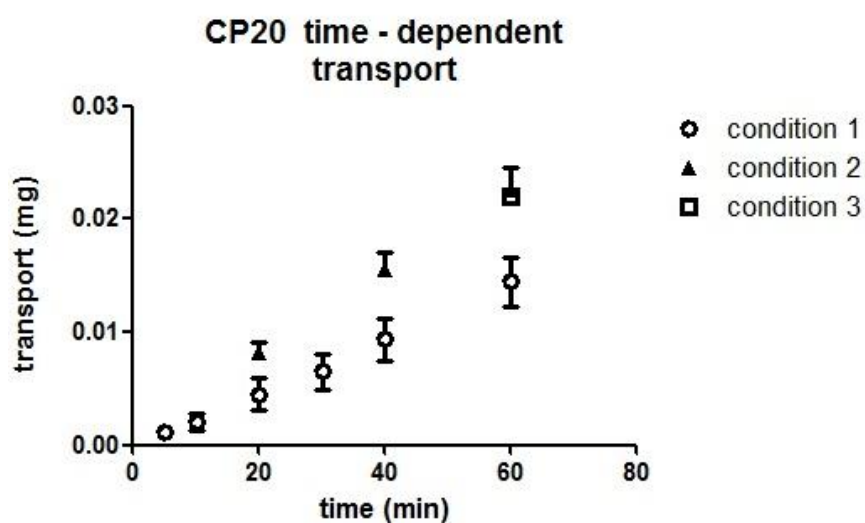


**Figure 18: Time dependent transfer of 800 $\mu$ M CP20 across the PBEC monolayer.**

**Transfer of CP20 is expressed in mg for 3 experimental conditions (explanation in the text).**

**Data is represented as mean  $\pm$  SEM (n=3).**

The time-dependent transport of CP20 almost follows a straight line as shown in Figure 18, which may suggest that CP20 transport across the PBEC monolayer is via non-facilitated diffusion.

After 20min  $6.36 \pm 2.02\%$  of CP20 were determined in the basolateral chamber for PBECs under experimental condition 1 and  $11.79 \pm 1.23\%$  for PBECs under experimental condition 2. After 40min, the amount of CP20 transferred was  $13.30 \pm 2.61\%$  and  $22.13 \pm 2.18\%$  for conditions 1 and 2 respectively.

After 60min,  $20.60 \pm 3.06\%$  of CP20 was transferred into the basolateral chamber for PBECs in experimental condition 1, whereas similar concentrations were found for conditions 2 and 3 ( $32.32 \pm 2.79\%$  and  $31.31 \pm 0.28\%$  respectively).

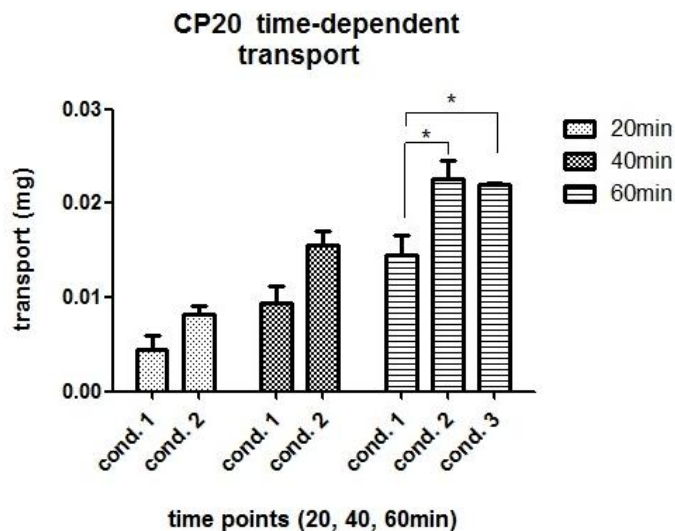


**Figure 19: Transfer of CP 20 expressed in mg, for the 3 experimental conditions (explanation in the text) after 20min, 40min and 60min.**

Data is represented as mean  $\pm$  SEM (n=3).

\*  $p < 0.05$

Moving the Transwell® inserts during the permeability assay was found to affect the transport of CP20 across the PBEC monolayer, as the more the filter inserts were moved the more CP20 permeability decreased as seen in Figure 18 and Figure 19.

At 20min and 40min no statistically significant difference in CP20 transfer was found when comparing experimental condition 1 and 2. However, after 60min, when the filter inserts were moved for the sixth time in case of PBECs in experimental condition 1, a significant difference was observed between conditions 1 and 2, as well as when comparing the experimental conditions 1 and 3.

These results confirmed that there is sufficient transfer of CP20 into the basolateral chamber after an assay time of 20min, hence 20min could be used as the end time point for the *in vitro* permeability assays.

Furthermore, these results suggested that the permeability assays should be conducted without any moving of the Transwell® inserts to reduce variability and therefore all further experiments were carried out using only a single end time point.

### 3.3 Relationship between TEER and sodium fluorescein permeability

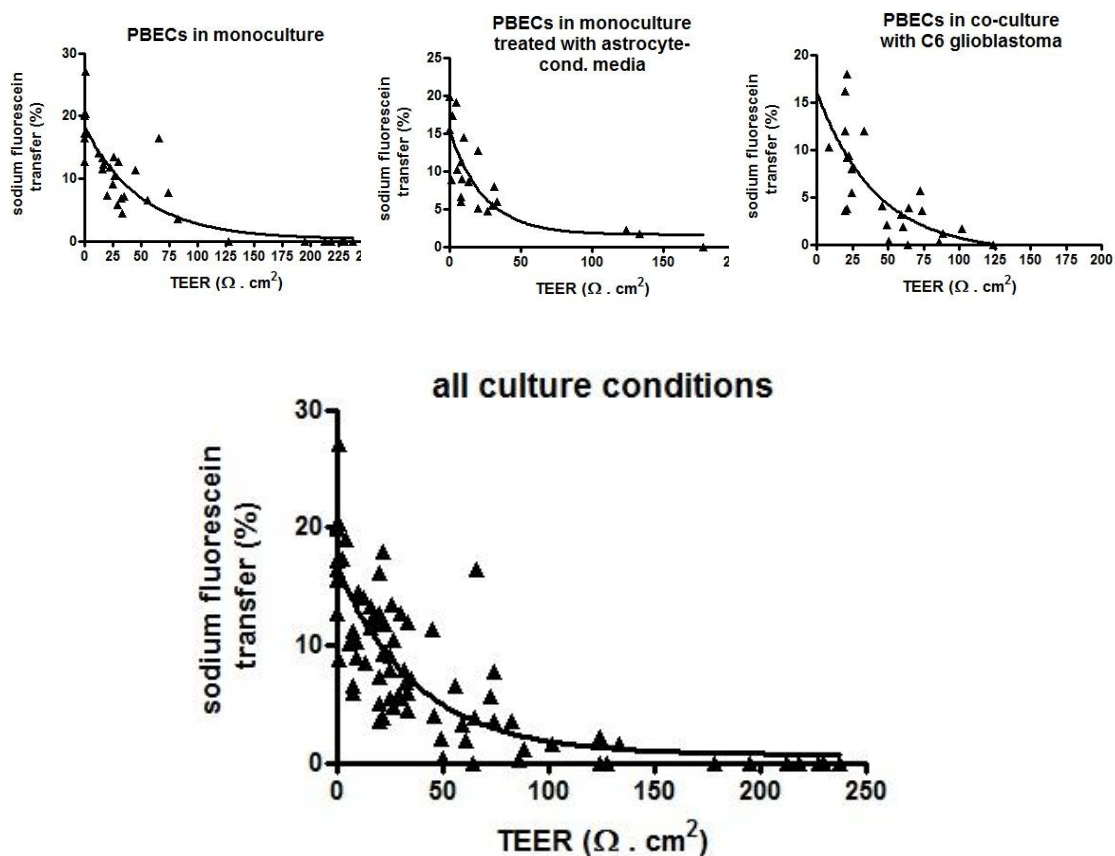


**Figure 20: Relationship between TEER and sodium fluorescein transfer with fitted curves for each of the 3 culture conditions and for the pooled data from all culture conditions (n=78).**

The relationship between the value of TEER and the permeability of the paracellular marker sodium fluorescein could be shown to be non-linear (Figure 20), as has been described in the literature by Gaillard and de Boer (2000). This becomes evident when looking at what influences the permeability of sodium fluorescein and the value of TEER. Transport of solutes depends on the sum of transport across all junctional pathways, therefore areas with leakier tight junctions will be averaged out by areas with tighter tight junctions. Contrary to that, in the case of the electrical resistance over the monolayer (TEER), the value is essentially determined by areas with the lowest resistance, even though these areas exist at a lower density (Gaillard and de Boer, 2000).

### 3.4 Influence of the culture condition

PBECs were grown under 3 different culture conditions (2.2.3.1) and the effect of the culture condition on the quality of the monolayer was investigated. For this purpose the differences in the value of TEER and the permeability of the paracellular marker sodium fluorescein were assessed.

#### 3.4.1 Influence on TEER

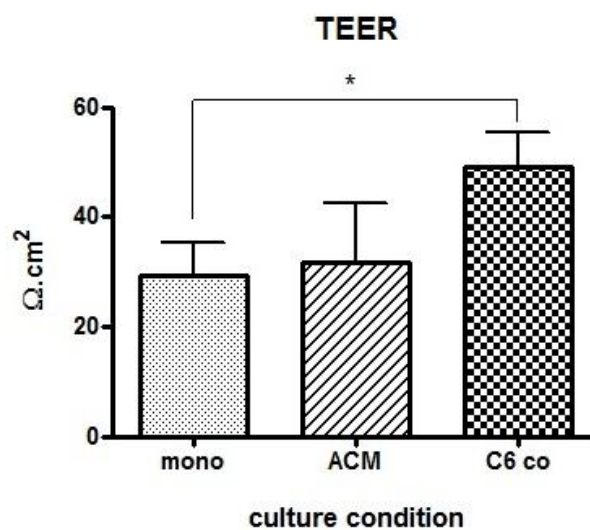


**Figure 21: Electrical resistance over the PBEC monolayer expressed in  $\Omega.cm^2$ , shown for each of the 3 culture conditions:**

**mono** PBECs grown in monoculture

**ACM** PBECs grown in monoculture and treated with astrocyte-conditioned media

**C6 co** PBECs grown in co-culture with C6 glioblastoma

Data is represented as mean  $\pm$  SEM (n=22-27).

Difference from control: \* p < 0.05

PBECs treated with astrocyte-conditioned media and PBECs grown in co-culture with C6 glioblastoma showed improved electrical resistance over the PBEC monolayer compared to PBECs that were grown in monoculture (Figure 21). PBECs in monoculture displayed TEER values of  $29.41 \pm 5.82 \Omega.cm^2$ , whereas PBECs in monoculture, that had additionally been treated with astrocyte-conditioned media, displayed TEERs of  $31.79 \pm 10.79 \Omega.cm^2$ . Co-culture with C6 glioblastoma affected electrical resistance the

most, as it increased by 67% to  $49.19 \pm 6.29 \Omega \cdot \text{cm}^2$  compared to PBECs grown in monoculture.

### 3.4.2 Influence on sodium fluorescein permeability

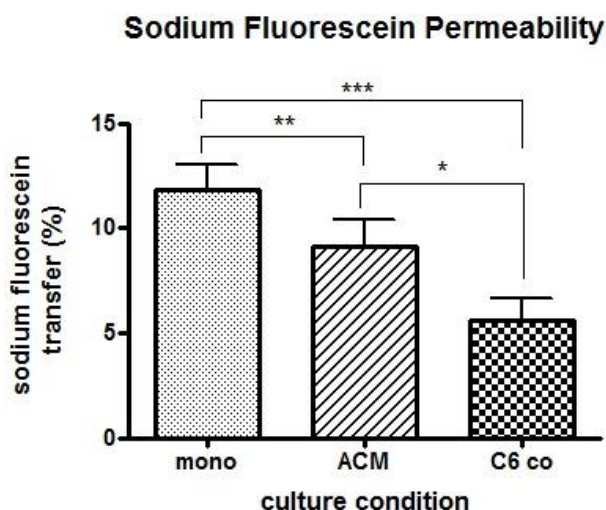


**Figure 22: Sodium fluorescein permeability in percent, shown for each of the 3 culture conditions:**

**Mono** PBECs grown in monoculture

**ACM** PBECs grown in monoculture and treated with astrocyte-conditioned media

**C6 co** PBECs grown in co-culture with C6 glioblastoma

Data is represented as mean ± SEM (n=22-27).

\* p < 0.05 / \*\* p < 0.01 / \*\*\* p < 0.001

Treatment with astrocyte-conditioned media as well as co-culture with C6 glioblastoma was found to effect sodium fluorescein permeability of the PBEC monolayer (Figure 22). Both conditions significantly decreased sodium fluorescein permeability compared to PBECs grown in monoculture. PBECs in monoculture demonstrated a sodium fluorescein transfer of  $11.85 \pm 1.16\%$ , whereas PBECs that had been treated with astrocyte-conditioned media showed a sodium fluorescein permeability of  $9.16 \pm 1.23\%$ . The greatest effect was found for PBECs grown in co-culture with C6 glioblastoma, where sodium fluorescein transfer decreased by 52% to a permeability of  $5.63 \pm 1.04\%$  compared to sodium fluorescein permeability of PBECs grown in monoculture.

## 3.5 Permeability assay

### 3.5.1 HPO transfer

Transfer of 800 $\mu$ M HPO from the apical to the basolateral chamber across the PBEC monolayer was studied in the permeability assay and HPO concentrations were determined after 20mins using HPLC. After analysis of the data, monolayers with TEER values below 40  $\Omega$ .cm<sup>2</sup> were considered not high enough and consequently excluded from the following data. The average TEER value of PBEC monolayers represented in the graphs below was 81.48  $\Omega$ .cm<sup>2</sup>.

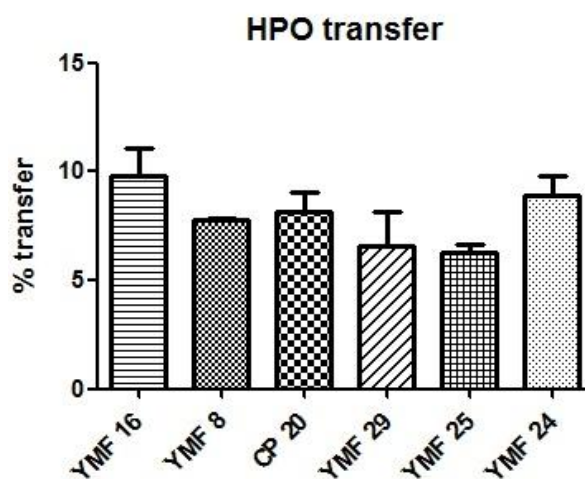


Figure 23: HPO overall transfer in percent across the PBEC monolayer (further explanation in the text).

Data is pooled from all culture conditions and represented as mean  $\pm$  SEM (n=2-5).

The overall transfer across the PBEC monolayer is expressed in percent and shown in Figure 23. This includes transfer into the basolateral chamber via the transendothelial cellular route as well as transfer via the paracellular route. Thus, HPO transfer had to be corrected for paracellular movement due to leaky tight junctions using the data acquired from the permeability of the paracellular marker sodium fluorescein. As a result of that, the data for corrected HPO transfer is shown in Figure 24.

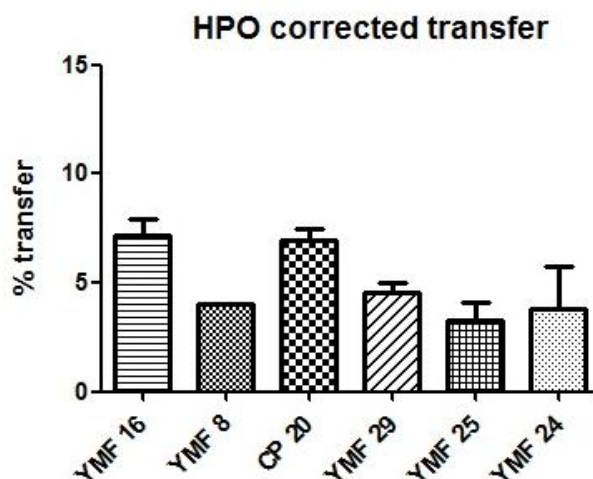


Figure 24: HPO transfer across the PBEC monolayer corrected for paracellular transport, expressed in percent (further explanation in the text).

Data is pooled from all culture conditions and represented as mean  $\pm$  SEM (n=2-5).

All HPOs were able to cross the blood-brain barrier in the *in vitro* assay. Compounds YMF 16 and CP20 showed the highest *in vitro* BBB permeability with  $7.17 \pm 1.36\%$  and  $6.98 \pm 1.05\%$  respectively. YMF 25 demonstrated the lowest ability to cross the PBEC monolayer with a permeability of  $3.31 \pm 1.34\%$ . Nevertheless, statistically no significant difference was found between the permeability of these HPOs.

### 3.5.2 *In vivo* – *in vitro* correlation

The aim of this study was to investigate whether a correlation between *in vitro* and *in vivo* blood-brain barrier permeability could be established, that would allow predictions of *in vivo* permeability to be made from *in vitro* data. For this purpose the data acquired from the *in vitro* permeability assays was plotted against *in vivo* permeability determined by Roy (2009).



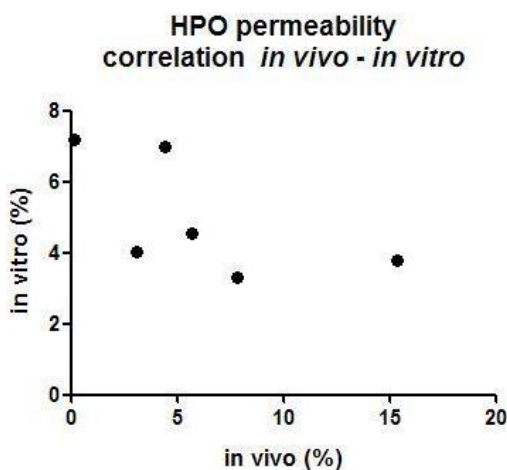


Figure 25: Correlation between *in vivo* and *in vitro* HPO blood-brain barrier permeability.

There was no correlation found between *in vivo* and *in vitro* HPO blood-brain barrier permeability ( $R^2 = 0.38$ ) (Figure 25).

### 3.5.3 Intracellular accumulation

In addition to determining HPO concentrations in the basolateral chamber after 20min, HPO concentrations in the apical chamber was also quantified in order to calculate intracellular accumulation.

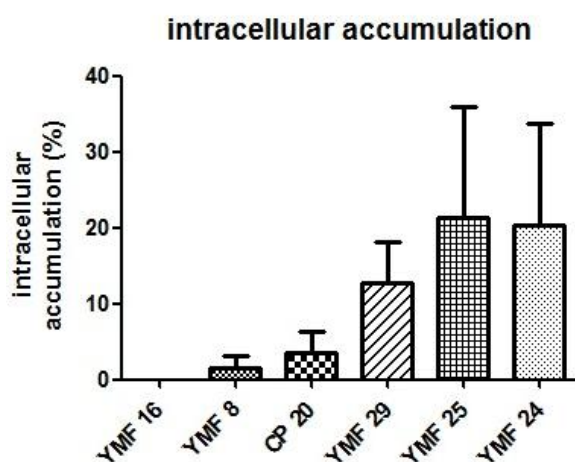


Figure 26: Calculated intracellular HPO accumulation in percent.

Data is pooled from all culture conditions and represented as mean  $\pm$  SEM (n=2-5).

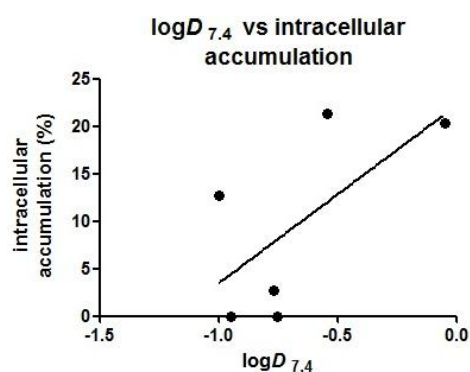


Figure 27: Correlation between calculated intracellular accumulation and  $\log D_{7.4}$ .  $R^2 = 0.43$

Despite the lack of a statistically significant difference between the intracellular accumulation of the HPOs (Figure 26), a trend ( $R^2 = 0.43$ ) could be observed when intracellular accumulation was plotted against the lipophilicity ( $\log D_{7.4}$ ) of the HPOs (Figure 27).

### 3.5.4 Transfer + intracellular accumulation and *in vivo* – *in vitro* correlation

Taking into account the trend observed in intracellular accumulation between the HPOs, values of intracellular accumulation were added to values of transfer across the PBEC monolayer to be able to better distinguish between the HPOs. As a result, transfer added to intracellular accumulation served as a measure of their ability to penetrate into and across the PBECs in the *in vitro* permeability assay.

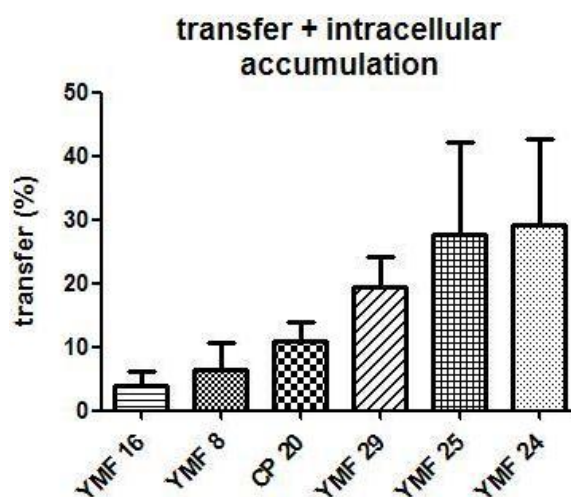
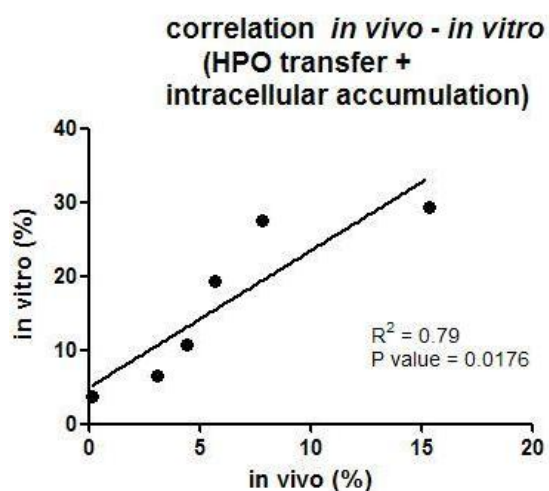


Figure 28: Combined values of HPO transfer and calculated intracellular accumulation in percent.

Data is pooled from all culture conditions and represented as mean  $\pm$  SEM (n=2-5).

The data for the combined values of intracellular accumulation and transfer across the monolayer is shown in Figure 28. The order of the HPOs changed greatly compared to their order in the data for HPO transfer alone (Figure 24). According to the combined data, compounds YMF 24 and YMF 25 demonstrated the highest ability to penetrate into and across the PBEC monolayer, whereas compound YMF 16 showed the lowest.



**Figure 29: Correlation between *in vitro* (transfer + intracellular accumulation) and *in vivo* HPO transfer.**

The combined data was then plotted against HPO *in vivo* permeability, where a good correlation between the combined *in vitro* data and the *in vivo* data could be established with a  $R^2$  of 0.79 and a p value of 0.0176.

### 3.5.5 Permeability vs. $\log D_{7.4}$ and MW

Since the physicochemical properties of a compound essentially influence its ability to cross the blood-brain barrier, the effects of molecular weight and lipophilicity ( $\log D_{7.4}$ ) on blood-brain barrier permeability of the HPOs used in this study was evaluated for both *in vitro* and *in vivo* data. The combined value of transfer across the endothelial cell monolayer added to calculated intracellular accumulation was used as the *in vitro* permeability.

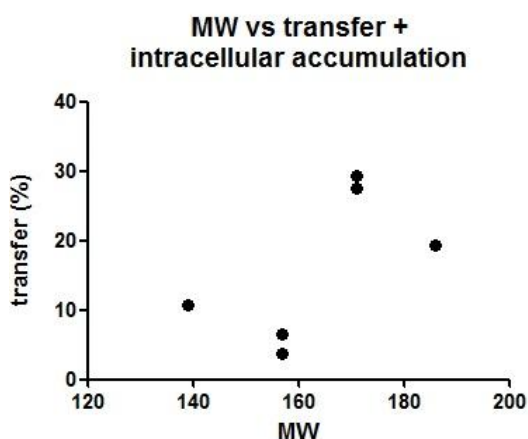


Figure 30: Molecular weight (MW) plotted against *in vitro* HPO transfer added to intracellular accumulation (expressed in percent).

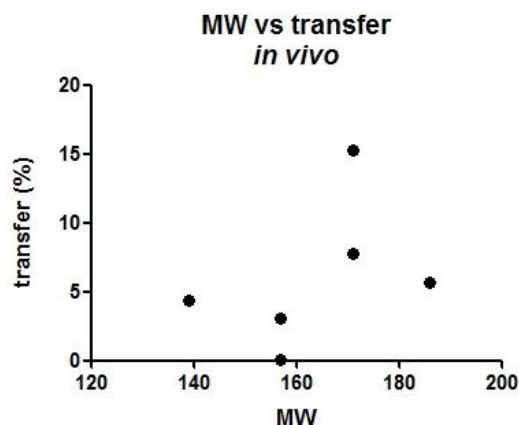


Figure 31: Molecular weight (MW) plotted against *in vivo* HPO transfer (expressed in percent).

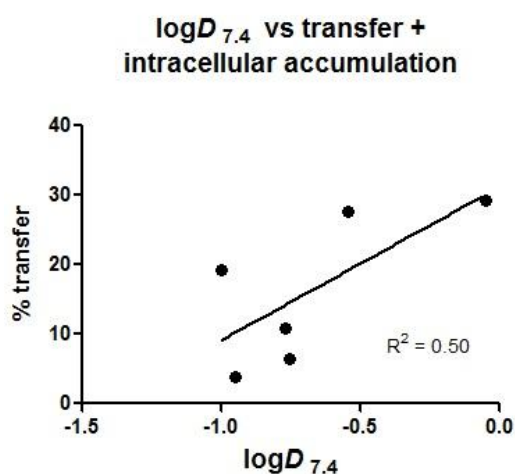


Figure 32:  $\log D_{7.4}$  plotted against *in vitro* HPO transfer added to intracellular accumulation (expressed in percent).

$R^2 = 0.50$

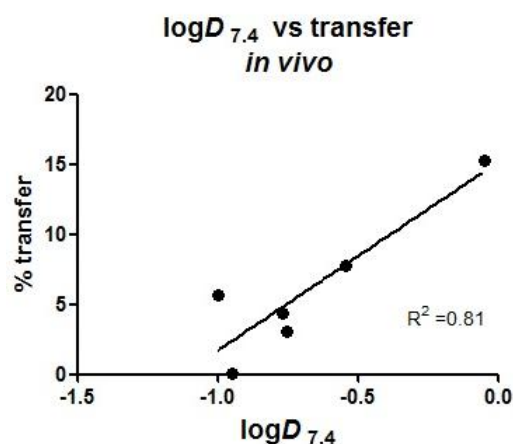


Figure 33:  $\log D_{7.4}$  plotted against *in vivo* HPO transfer (expressed in percent).

$R^2 = 0.81$

There was no correlation found between the molecular weight of the HPOs and the blood-brain barrier permeability, neither in the case of the *in vitro* nor the *in vivo* data (Figure 30, Figure 31). Contrary to the molecular weight, a correlation between the  $\log D_{7.4}$  and the blood-brain barrier permeability was confirmed for the HPOs used in this study. *In vivo* blood-brain barrier permeability data correlated significantly with  $\log D_{7.4}$  of the HPOs with  $R^2 = 0.81$  (Figure 33) compared to the *in vitro* correlation with  $R^2 = 0.50$  (Figure 32).

### **3.6 HPLC**

The HPOs showed a single, sharp peak in the chromatogram with retention times between 10-13min. Sample chromatograms and standard curves for all HPOs are shown in the appendix (9.1, 9.2).

Compound YMF 29 showed 3 separate peaks in its chromatogram, therefore mass spectrometry (MS) was applied to investigate whether this was the result of compound degradation. MS confirmed that YMF 29 had not degraded (spectrum shown in appendix 9.3), thus the biggest peak at a retention time of 10min was used to base the standard curve upon and to calculate concentrations from the permeability assay samples.

## 4 DISCUSSION

Iron chelation therapy is a promising new therapeutic approach in the treatment of neurodegenerative diseases like Parkinson's disease, Alzheimer's disease or Friedreich's Ataxia. Hydroxypyridinones (HPOs) have been identified as suitable iron chelators and the orally active iron chelator CP20 (deferiprone) has already been shown to be able to cross the blood-brain barrier (BBB) (Hider et al., 2011). Hence analogues of CP20 were synthesized and *in vivo* experiments were carried out on guinea pigs using the in situ brain perfusion technique to determine BBB permeability of these HPOs (Roy, 2009).

Although *in vivo* experiments provide valuable information, the fact that they are both cost and labour intensive fuel the search for other models to test BBB permeability. Thus, an *in vitro* assay could represent a good alternative to *in vivo* experiments. In addition, an *in vitro* assay would potentially allow for predictions of *in vivo* BBB permeability to be made from the *in vitro* data. Consequently, an *in vitro* assay could serve as an initial screening in the process of designing and synthesizing new HPOs.

To develop such an *in vitro* assay, primary porcine brain endothelial cells were used in this study. Furthermore, the same concentration (800 $\mu$ M), as well as the same end time point (20min), that had been used to perform the *in vivo* experiments, was applied in order to accurately compare the *in vitro* and *in vivo* data.

### 4.1 *In vitro* system

A good BBB *in vitro* model should represent the situation found *in vivo* as closely as possible in regard to the specific characteristics of the BBB (1.2.2). When performing transport studies, the formation of a sufficiently tight monolayer, which expresses high electrical resistance and a low permeability to marker molecules, is the primary goal in the establishment of the BBB *in vitro* model. However, the loss of characteristic properties of primary brain endothelial cells when cultured *in vitro* presents a problem and various approaches have been studied to enhance tight junction formation including the use of hydrocortisone, serum free media, cAMP and the influence of astrocytes (Hoheisel et al., 1998; Rubin et al., 1991).

Therefore, the influence of different culture conditions on the integrity of the PBEC monolayer was investigated in this study. PBECs were subjected to 3 different culture

conditions, as they were either grown in monoculture, in the presence of astrocytic factors (astrocyte-conditioned media (ACM), taken from cultured primary rat astrocytes) or in non-contact co-culture with C6 glioblastoma. PBECs grown in monoculture served as a control to evaluate the results. As shown in the results (3.4), TEER for PBECs treated with ACM increased by 8% while co-culture with C6 glioblastoma increased the value of TEER by 67%. In addition, the permeability of sodium fluorescein could be significantly decreased by 22% in the case of PBECs treated with astrocyte conditioned media and 52% in the case of PBEC/C6 glioblastoma co-culture.

These results show that astrocytes influence the barrier properties *in vitro* and tightness of the barrier can be improved by using conditioned media or co-culture. However, co-culture with C6 glioblastoma was found to have a greater effect on both the value of TEER and the permeability of sodium fluorescein, suggesting that the influence of astrocytes on barrier integrity is not only mediated by soluble factors. A close contact that allows for constant interchange seems to further positively affect the quality of the monolayer in regard to tight junction formation. Thus, the closer the culture conditions are to conditions present *in vivo*, the better the tight junctions are at restricting paracellular movement across the PBEC monolayer, represented by an increase in TEER and a decrease in sodium fluorescein permeability.

These findings are in general agreement with other published studies, though the degree of improved barrier tightness varied between the present study and the previously published ones, but also varied greatly among the published data. For example, Zhang et al. (2006) found that PBECs treated with ACM from primary astrocytes increased the TEER by 10-25% and Smith et al. (2007) showed that PBECs treated with ACM from C6 glioblastoma resulted in an increase in TEER by a factor of 5 and co-culture with C6 glioblastoma by a factor of 10. The average TEER displayed by PBECs used for experiments in this study was  $81.48 \Omega \cdot \text{cm}^2$ . However, Franke et al. (2000) developed a model with PBECs that reached TEERs of  $700 \Omega \cdot \text{cm}^2$ , peak resistance even reached  $1500 \Omega \cdot \text{cm}^2$ , without the influence of astrocytes. Zhang et al. (2006) also reported higher TEER values ( $300\text{-}550 \Omega \cdot \text{cm}^2$ ) when PBECs were treated with ACM. Contrary to these findings, in the study of Jeliazkova-Mecheva and Bobilya (2003), PBECs grown in monoculture reached average TEERs of only  $28 \Omega \cdot \text{cm}^2$ , but TEER value could be increased when PBECs received treatment with ACM to above  $100 \Omega \cdot \text{cm}^2$ .

Keeping in mind that transport studies are aimed to be performed on the PBEC monolayers, a sufficiently tight barrier needs to be formed in order to accurately distinguish between low permeability compounds. Gaillard and de Boer (2000) showed that the relationship between the value of TEER and the permeability of sodium fluorescein was not linear. Monolayers with a TEER value above  $131 \Omega \cdot \text{cm}^2$  were determined suitable for performing transport experiments, since above this value, sodium fluorescein permeability was shown to be independent of a further increase in TEER. This non-linear relationship was also observed in the present study (Figure 20), but the threshold value of  $131 \Omega \cdot \text{cm}^2$  could not be reached for the majority of the monolayers. However, monolayers used for the first experiments with CP20 (time-dependent transport) reached peak resistances of up to  $240 \Omega \cdot \text{cm}^2$ .

Interestingly, CP20 permeability in these experiments was 9.08% compared to 6.98% in the permeability assays performed afterwards with PBEC monolayers that displayed much lower TEERs (average TEER used for experiments with CP20:  $107 \Omega \cdot \text{cm}^2$ ) and a much higher sodium fluorescein permeability (negligible sodium fluorescein permeability in the time-dependent experiments with CP20). This suggests that correcting the permeability value for paracellular transport using the sodium fluorescein data, may be a good approach to correct for leakier tight junctions, since statistically (unpaired, two tailed t-test) these results are not different from the results obtained from PBEC monolayers, which demonstrated sufficient TJ formation for performing experiments.

Although these results lack statistical difference, correcting data from PBEC monolayers with leaky tight junctions apparently underestimated the permeability of CP20. When monolayers don't form tight TJ (high sodium fluorescein permeability), it cannot be guaranteed that exactly the same fraction of CP20 is transferred into the basolateral chamber via the paracellular route as is the case for sodium fluorescein, where the only known route of transfer into the basolateral chamber is the paracellular one. Therefore it seems reasonable that a correction based on this assumption could easily overestimate the paracellular proportion of CP20 transport and hence underestimate the "real" transfer, which is via the transendothelial cellular route. Consequently, future work should be directed towards being able to cultivate PBECs with sufficiently tight monolayers and thus negligible sodium fluorescein permeability.

Despite this, the underlying problem of culturing primary brain endothelial cells remains -



batch to batch reproducibility. Biological variations and tissue quality are one of the main obstacles when developing a reproducible BBB *in vitro* model, considering that every brain used to isolate endothelial cells is different from the next. This may explain the low TEER values demonstrated by the PBECs used for this study, since in the same research group PBECs from previous isolations displayed TEERs of up to 800  $\Omega\cdot\text{cm}^2$ .

## 4.2 *In vivo* – *in vitro* correlation

Apart from the problems encountered with primary cell culture, future work might have to focus on improving the *in vitro* assay as well. The main objective for this study was to develop an *in vitro* assay to make it possible to correlate *in vivo* and *in vitro* data. However, no correlation was found when *in vivo* and *in vitro* permeability was plotted (Figure 25). Interestingly, a difference in intracellular accumulation between the HPOs was found and, despite the lack of a statistically significant difference, a trend could be observed when intracellular accumulation and lipophilicity ( $\log D_{7.4}$ ) were plotted (Figure 27). This suggests that the higher the lipophilicity of the HPO, the more it was retained in the cell monolayer. Since penetrating into the endothelial cells is the first step for the HPOs to cross the endothelial cell layer (blood-brain barrier) and reach the basolateral chamber (brain), this observation was essential. Therefore, the values of intracellular accumulation were added to the values of transfer across the PBEC monolayer and subsequently served as a measure of their ability to penetrate into and across the PBEC monolayer. As a result, it was possible to establish a good correlation ( $R^2 = 0.79$ ) between the *in vivo* and *in vitro* blood-brain barrier permeability (Figure 29). Thus, a longer end time point might be needed when performing the *in vitro* assay in order to ensure that the HPOs retained in the cell layer are able to cross into the basolateral chamber.

Moreover, the effect of the unstirred water layer *in vitro* may have to be considered since *in vivo* there is virtually no unstirred water layer due to a mixing effect of circulating erythrocytes (Youdim et al, 2003). On the contrary, the unstirred water layer present in *in vitro* experiments has been shown to influence *in vitro* permeability, as it can be a rate limiting factor (Avdeef, 2010; Zhang et al., 2006). As a consequence, the *in vitro* assays may have to be carried out at stirring rate higher than 200rpm, which was used during the experiments in this study, as for example Zhang et al. (2006) applied 600rpm. However,

when applying higher stirring rates, the fragility of primary endothelial cells needs to be considered carefully (Avdeef, 2010). Thus, there is a need of further research in order to determine a stirring rate that sufficiently decreases the effect of the unstirred water layer but at the same time does not affect the barrier integrity.

### 4.3 Influence of structural features on BBB permeability

The HPOs used in this study were designed as close analogues of deferiprone (CP20) with regard to oral availability and iron chelation ability, but with the aim to have an enhanced BBB permeability. The effect of increasing molecular weight (longer N-alkyl substitution) and the introduction of a fluorine atom on the pyridine ring were to be investigated (Roy, 2009).

It was found that lipophilicity correlated with BBB permeability, both *in vitro* and *in vivo* (Figure 32, Figure 33), but no correlation was found between the molecular weight and BBB permeability. This might be due to a limited range of molecular weights displayed by the HPOs selected for this study (Table 1). When looking closely at the structures of the selected HPOs, interesting observations can be made. Compounds YMF 8 and YMF16, as well as compounds YMF 24 and YMF 25 have the same molecular weight, but differ in the position of the fluorine atom on the pyridinone ring. In the case of YMF 8 and YMF 24, the pyridinone ring is substituted with the fluorine at position 2, whereas in the case of YMF 16 and YMF 25 the fluorine is at position 5 of the pyridinone ring. It was found that the position of the fluorine on the ring affected lipophilicity ( $\log D_{7.4}$ ) and may subsequently also influence BBB permeability.

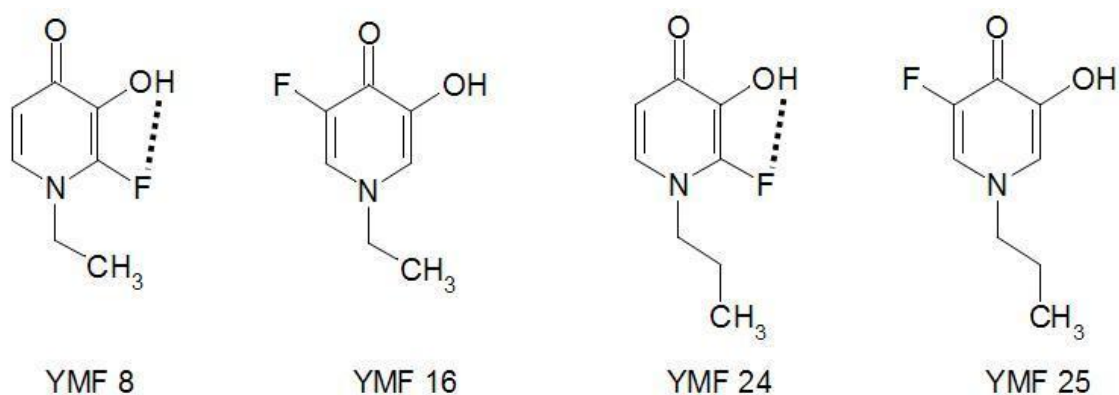
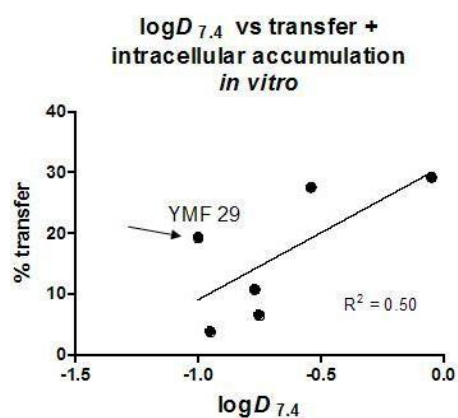


Figure 34: Structure of YMF 8, YMF 16, YMF 24 and YMF 25. Intramolecular hydrogen bonds shown for YMF 8 and YMF 24

An intramolecular hydrogen bond is most likely able to form between the fluorine in position 2 and the 3-hydroxyl hydrogen (Figure 34). This causes the fluorine to be less available for hydrogen bonding with the solvent, subsequently making these HPOs more lipophilic compared to HPOs with fluorine substitution in position 5. This effect may be responsible for the higher BBB permeability found for YMF 8 and YMF 24 compared to YMF 16 and YMF 25 respectively.

Furthermore, it is noticed that YMF 29 was found to have a higher BBB permeability than would be predicted from its  $\log D_{7.4}$ . This observation could be made for the *in vitro* (Figure 35) data, but more clearly for the *in vivo* data (Figure 36).



**Figure 35:**  $\log D_{7.4}$  plotted against HPO *in vitro* transfer added to intracellular accumulation (expressed in percent). The arrow points out the dot that represents YMF 29.

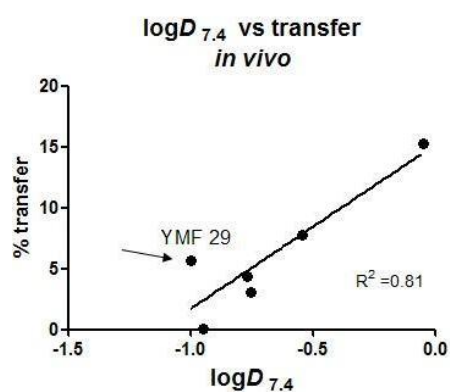


**Figure 36:**  $\log D_{7.4}$  plotted against HPO *in vivo* permeability (expressed in percent). The arrow points out the dot that represents YMF 29.

Structurally, YMF 29 differs from the other CP20 analogues. An additional amide moiety was introduced to the pyridinone ring at position 5, though YMF 29 also has a fluorine substitution at position 2, like YMF 8 and YMF 24. This amide substitution is responsible for YMF 29 hydrophilic properties, however, it may also be responsible for the enhanced ability of YMF 29 to cross the BBB compared to the more lipophilic HPOs. Its high BBB permeability in regard to its lipophilicity, is most likely due to an intramolecular hydrogen bond that can be formed between the amide functionality and the carbonyl oxygen (Figure 37).

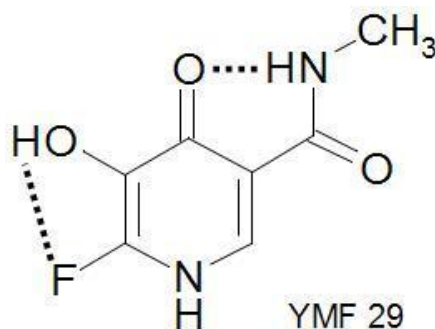


**Figure 37: Structure and intramolecular hydrogen bonds of YMF 29**

Moreover, the fluorine in position 2 may be able to form an intramolecular hydrogen bond with the 3-hydroxy hydrogen as discussed for YMF 8 and YMF 24. The fact that both hydrogen atoms, otherwise available for intermolecular hydrogen bonding with other molecules, are involved in these intramolecular hydrogen bonds, positively influence the compounds ability to permeate membranes (Roy, 2009). Additionally, the intramolecular hydrogen bonds make YMF 29 completely planar, which further assists the compound in successfully crossing membranes. Consequently, when designing BBB permeable HPOs, structural features similar to those of YMF 29 could be useful.

#### 4.4 Toxicity and neuroprotection

Although BBB permeability is a key quality for HPOs that can potentially be used for the treatment of neurodegenerative diseases, the possibly toxic effects on endothelial cells, neurons and other brain cells must not be neglected. Moreover, the HPOs should provide neuroprotection against insults involving iron.

In order to determine the effect of HPOs on endothelial cell viability, toxicity assays were performed on PBECs and the results showed that YMF 8, YMF 16 and YMF 24 affected cell viability after 2 hours, with about 76-82% of cells remaining viable. For CP20 no toxic effect on PBECs was found. For the treatment of transfusional iron overload in patients suffering from  $\beta$ -Thalassaemia, CP20 (deferiprone) is administered at a concentration of 25-100mg/kg (180-720 $\mu$ M) (Hoffbrand et al., 2003), which is lower compared to the concentration used in the present study (800 $\mu$ M). In a previous study, toxicity assays using mouse embryonic cortical neurons showed that neither CP20 nor YMF 24, YMF 25 or YMF 29 had an effect on neuronal cell viability at the

concentrations of 10 $\mu$ M, 30 $\mu$ M and 100 $\mu$ M over an incubation time of 24 hours (Roy, 2009). The concentrations used on the cortical neurons, again were much lower than the concentration used on PBECs, though the incubation time was longer. Consequently, there may be a need for further investigation on the toxicity of the CP20 analogues on PBECs.

What is more, in a recent study, the neuroprotective abilities against various insults (ferric nitrilotriacetate, H<sub>2</sub>O<sub>2</sub> and A $\beta$ (1-40)) on cultured cortical neurons could be shown for CP20 (Molina-Holgado et al., 2008). Moderate ability to demonstrate neuroprotection against these insults was found for YMF 24 and YMF 25, whereas superior to equal neuroprotective efficiency was demonstrated for YMF 29 compared to CP20 (Roy, 2009).

## 4.5 Clinical use

In a clinical trial with patients suffering from Friedreich's Ataxia, CP20 (deferiprone) was shown to demonstrate beneficial effects (Boeddard et al., 2007). Moreover, deferiprone is currently under investigation in a clinical trial for the treatment of Parkinson's disease.

Due to their small size and non-charged nature, the HPOs can cross the BBB and the route of transfer is most likely passive diffusion (Hider et al., 2011), which could also be observed in the present study (Figure 18). However, non-facilitated diffusion clearly limits the maximum flux of the HPO into the brain, which may require a more efficient targeting mechanism in order to enhance their BBB permeability (Hider et al., 2011). A potential approach could be the use of nanoparticles, which can use different address systems such as the melanotransferrin receptor, the transferrin receptor and the apolipoprotein receptor. These nanoparticles may also be able to recross into the bloodstream, but on the other hand would have to be administered parenterally (Hider et al., 2011).

An alternative approach to enhance BBB permeability could be the use of sugar conjugates, which would make it possible to administer the drug orally. The fact that there is a high expression of the glucose transporter GLUT-1 at the BBB would facilitate the entry of the HPO-sugar conjugate into the brain. Moreover, its hydrophilic properties would limit liver first pass effects. Despite this, the O-glycosylated deferiprone was found not to cross the BBB in a recent study (Roy et al., 2010).

## 5 ABSTRACT

Oxidative stress and protein aggregation have been shown to play a key role in the pathology of neurodegenerative diseases like Alzheimer's disease and Parkinson's disease. Moreover, high levels of metals like iron have been found to accumulate in the brain, which may provide the link between oxidative stress, protein aggregation and neurodegeneration. Iron chelation is a promising new therapeutic strategy for the treatment of these diseases and 3-hydroxypyridin-4-ones (HPO) have been identified as suitable chelators. In order to chelate the labile iron present in the brain, the iron chelator must be able to cross the blood-brain barrier (BBB), rendering the assessment of BBB permeability an essential task. Since *in vivo* experiments are both labour and cost intensive, an *in vitro* assay could serve as a good alternative. Thus, the aim of this study was to develop an *in vitro* assay to determine the BBB permeability of the selected HPOs and to correlate the acquired *in vitro* data with *in vivo* data that was already available. Such a correlation would then allow for predictions of *in vivo* BBB permeability to be made from *in vitro* data, which could be quite beneficial in the process of designing and synthesizing new HPOs. Primary porcine brain endothelial cells (PBEC) were used in this study and transport across the cell monolayer was studied using a Transwell® system. PBECs were subjected to 3 different culture conditions in order to evaluate different approaches to enhance barrier integrity *in vitro*. Moreover, the effect of the HPOs on PBEC viability was investigated. All the selected HPOs were able to cross the BBB *in vitro* and a good correlation was found between the *in vitro* and the *in vivo* BBB permeability, when HPO transfer added to the value of intracellular accumulation was used as a measure of *in vitro* BBB permeability.

## 6 ZUSAMMENFASSUNG

Oxidativer Stress und Proteinaggregation spielen eine wichtige Rolle in der Pathogenese von neurodegenerativen Erkrankungen wie der Alzheimer- und der Parkinson- Krankheit. Darüber hinaus konnte die Akkumulation von Metallen wie Eisen im Gehirn von Erkrankten nachgewiesen werden, was möglicherweise den Zusammenhang zwischen oxidativem Stress, Proteinaggregation und Neurodegeneration herstellt. Eisenchelation ist daher eine neue, vielversprechende therapeutische Strategie um diese Krankheiten zu behandeln und 3-Hydroxypyridin-4one (HPO) stellen passende Chelatoren für diese Anwendung dar. Um das labile Eisen im Gehirn zu chelatieren, muss der Eisenchelator die Fähigkeit besitzen, die Blut-Hirnschranke zu überwinden. Daher ist das Bestimmen der Blut-Hirnschranken-Permeabilität ein wichtiger Schritt. *In vitro* Experimente könnten hierbei eine gute Alternative zu arbeits- und kostenintensiven *in vivo* Experimenten darstellen. Demzufolge war das Ziel dieser Diplomarbeit einen *in vitro* Assay zu entwickeln, um die Blut-Hirnschranken-Permeabilität von ausgewählten HPOs zu bestimmen und diese mit schon vorhandenen *in vivo* Daten zu korrelieren. Solch eine Korrelation würde das Vorhersagen von *in vivo* Permeabilität an Hand von *in vitro* Daten ermöglichen, was besonders für die Entwicklung und Synthese von neuen HPOs vorteilhaft wäre. Primäre porcine Gehirn-Endothelzellen (PBEC) wurden für den *in vitro* Assay verwendet und der Transport der HPOs durch den Zellmonolayer mit Hilfe eines Transwell® Systems untersucht. Die PBECs wurden unter 3 verschiedenen Bedingungen kultiviert, um die Evaluierung verschiedener Methoden zur Verbesserung der Barrierenfunktion *in vitro* zu ermöglichen. Alle getesteten HPOs konnten im *in vitro* Assay die Blut-Hirnschranke überwinden. Eine gute Korrelation zwischen *in vitro* und *in vivo* Permeabilität konnte gezeigt werden, sobald HPO-Transfer addiert zu der Konzentration an intrazellulär verbleibenden HPOs als Maß für die *in vitro* Permeabilität herangezogen wurde.

## 7 REFERENCES

- Abbott, N. J. (2004). "Prediction of blood-brain barrier permeation in drug discovery from in vivo, in vitro and in silico models." *Drug Discovery Today: Technologies* 1(4): 407-416.
- Abbott, N. J., Patabendige, A. A., Dolman, D. E., Yusof, S. R. and Begley, D. J. (2010). "Structure and function of the blood-brain barrier." *Neurobiology of disease* 37(1): 13-25.
- Abbott, N. J., Ronnback, L. and Hansson, E. (2006). "Astrocyte-endothelial interactions at the blood-brain barrier." *Nature reviews. Neuroscience* 7(1): 41-53.
- Altamura, S. and Muckenthaler, M. U. (2009). "Iron toxicity in diseases of aging: Alzheimer's disease, Parkinson's disease and atherosclerosis." *Journal of Alzheimer's disease* : JAD 16(4): 879-895.
- Avdeef, A. (2011). "How well can in vitro brain microcapillary endothelial cell models predict rodent in vivo blood-brain barrier permeability?" *European journal of pharmaceutical sciences : official journal of the European Federation for Pharmaceutical Sciences* 43(3): 109-124.
- Ballard, C., Gauthier, S., Corbett, A., Brayne, C., Aarsland, D. and Jones, E. (2011). "Alzheimer's disease." *Lancet* 377(9770): 1019-1031.
- Begley, D. J. (2004). "ABC transporters and the blood-brain barrier." *Current pharmaceutical design* 10(12): 1295-1312.
- Bernacki, J., Dobrowolska, A., Nierwinska, K. and Malecki, A. (2008). "Physiology and pharmacological role of the blood-brain barrier." *Pharmacological reports* : PR 60(5): 600-622.
- Bickel, U. (2005). "How to measure drug transport across the blood-brain barrier." *NeuroRx : the journal of the American Society for Experimental NeuroTherapeutics* 2(1): 15-26.
- Bobilya, D. J., D'Amour, K., Palmer, A., Skeffington, C., Therrien, N. and Tibaduiza, E. C. (1995). "Isolation and cultivation of porcine brain capillary endothelial cells as an in vitro model of the blood-brain barrier." *Methods in Cell Science* 17(1): 25-32.



- Boddaert, N., Le Quan Sang, K. H., Rötig, A., Leroy-Willig, A., Gallet, S., Brunelle, F., Sidi, D., Thalabard, J.-C., Munnich, A. and Cabantchik, Z. I. (2007). "Selective iron chelation in Friedreich ataxia: biologic and clinical implications." *Blood* 110(1): 401-408.
- Borst, P., Evers, R., Kool, M. and Wijnholds, J. (2000). "A family of drug transporters: the multidrug resistance-associated proteins." *Journal of the National Cancer Institute* 92(16): 1295-1302.
- Butt, A. M., Jones, H. C. and Abbott, N. J. (1990). "Electrical resistance across the blood-brain barrier in anaesthetized rats: a developmental study." *The Journal of physiology* 429(1): 47-62.
- Camaschella, C. and Strati, P. (2010). "Recent advances in iron metabolism and related disorders." *Internal and Emergency Medicine* 5(5): 393-400.
- Cardoso, F. L., Brites, D. and Brito, M. A. (2010). "Looking at the blood-brain barrier: molecular anatomy and possible investigation approaches." *Brain research reviews* 64(2): 328-363.
- Carvey, P. M., Hendey, B. and Monahan, A. J. (2009). "The blood-brain barrier in neurodegenerative disease: a rhetorical perspective." *Journal of neurochemistry* 111(2): 291-314.
- Cecchelli, R., Berezowski, V., Lundquist, S., Culot, M., Renftel, M., Dehouck, M. P. and Fenart, L. (2007). "Modelling of the blood-brain barrier in drug discovery and development." *Nature reviews. Drug discovery* 6(8): 650-661.
- Deli, M. A., Abraham, C. S., Kataoka, Y. and Niwa, M. (2005). "Permeability studies on in vitro blood-brain barrier models: physiology, pathology, and pharmacology." *Cellular and molecular neurobiology* 25(1): 59-127.
- Denizot, F. and Lang, R. (1986). "Rapid colorimetric assay for cell growth and survival. Modifications to the tetrazolium dye procedure giving improved sensitivity and reliability." *Journal of Immunological Methods* 89(2): 271-277.
- Eyal, S., Hsiao, P. and Unadkat, J. D. (2009). "Drug interactions at the blood-brain barrier: fact or fantasy?" *Pharmacology & Therapeutics* 123(1): 80-104.
- Franke, H., Galla, H. and Beuckmann, C. T. (2000). "Primary cultures of brain microvessel endothelial cells: a valid and flexible model to study drug transport through the blood-brain barrier in vitro." *Brain Research Protocols* 5(3): 248-256.

- Gaeta, A. and Hider, R. C. (2005). "The crucial role of metal ions in neurodegeneration: the basis for a promising therapeutic strategy." *British Journal of Pharmacology* 146(8): 1041-1059.
- Gaillard, P. J. and de Boer, A. G. (2000). "Relationship between permeability status of the blood-brain barrier and in vitro permeability coefficient of a drug." *European journal of pharmaceutical sciences: official journal of the European Federation for Pharmaceutical Sciences* 12(2): 95-102.
- Gille, G. and Reichmann, H. (2011). "Iron-dependent functions of mitochondria--relation to neurodegeneration." *Journal of Neural Transmission* 118(3): 349-359.
- Gumbleton, M. and Audus, K. L. (2001). "Progress and limitations in the use of in vitro cell cultures to serve as a permeability screen for the blood-brain barrier." *Journal of pharmaceutical sciences* 90(11): 1681-1698.
- Hawkins, B. T. and Davis, T. P. (2005). "The blood-brain barrier/neurovascular unit in health and disease." *Pharmacological reviews* 57(2): 173-185.
- Hentze, M. W., Muckenthaler, M. U., Galy, B. and Camaschella, C. (2010). "Two to tango: regulation of Mammalian iron metabolism." *Cell* 142(1): 24-38.
- Hider, R. C., Ma, Y., Molina-Holgado, F., Gaeta, A. and Roy, S. (2008). "Iron chelation as a potential therapy for neurodegenerative disease." *Biochemical Society Transactions* 36(Pt 6): 1304-1308.
- Hider, R. C., Roy, S., Ma, Y. M., Le Kong, X. and Preston, J. (2011). "The potential application of iron chelators for the treatment of neurodegenerative diseases." *Metallomics* 3(3): 239-249.
- Higgins, G. C., Beart, P. M., Shin, Y. S., Chen, M. J., Cheung, N. S. and Nagley, P. (2010). "Oxidative stress: emerging mitochondrial and cellular themes and variations in neuronal injury." *Journal of Alzheimer's disease : JAD* 20 Suppl 2: 453-473.
- Hoffbrand, A. V., Cohen, A. and Hershko, C. (2003). "Role of deferiprone in chelation therapy for transfusional iron overload." *Blood* 102: 17-24.
- Hoheisel, D., Nitz, T., Franke, H., Wegener, J., Hakvoort, A., Tilling, T. and Galla, H. J. (1998). "Hydrocortisone reinforces the blood-brain barrier properties in a serum free cell culture system." *Biochemical and biophysical research communications* 244(1): 312-316.

- Horowitz, M. P. and Greenamyre, J. T. (2010). "Mitochondrial iron metabolism and its role in neurodegeneration." *Journal of Alzheimer's disease* : JAD 20 Suppl 2: S551-568.
- Jeliazkova-Mecheva, V. V. and Bobilya, D. J. (2003). "A porcine astrocyte/endothelial cell co-culture model of the blood-brain barrier." *Brain Research Protocols* 12(2): 91-98.
- Jomova, K., Vondrakova, D., Lawson, M. and Valko, M. (2010). "Metals, oxidative stress and neurodegenerative disorders." *Molecular and cellular biochemistry* 345(1): 91-104.
- Kell, D. B. (2010). "Towards a unifying, systems biology understanding of large-scale cellular death and destruction caused by poorly liganded iron: Parkinson's, Huntington's, Alzheimer's, prions, bactericides, chemical toxicology and others as examples." *Archives of Toxicology* 84(11): 825-889.
- Kenche, V. B. and Barnham, K. J. (2011). "Alzheimer's disease & metals: therapeutic opportunities." *British Journal of Pharmacology* 163(2): 211-219.
- Leslie, E. M., Deeley, R. G. and Cole, S. P. (2005). "Multidrug resistance proteins: role of P-glycoprotein, MRP1, MRP2, and BCRP (ABCG2) in tissue defense." *Toxicology and applied pharmacology* 204(3): 216-237.
- Li, X., Jankovic, J. and Le, W. (2011). "Iron chelation and neuroprotection in neurodegenerative diseases." *Journal of Neural Transmission* 118(3): 473-477.
- Liu, D. Y., Liu, Z. D., Lu, S. L. and Hider, R. C. (1999). "Gradient ion-pair high-performance liquid chromatographic method for analysis of 3-hydroxypyridin-4-one iron chelators." *Journal of Chromatography B: Biomedical Sciences and Applications* 730(1): 135-139.
- Liu, Z. D. and Hider, R. C. (2002). "Design of clinically useful iron(III)-selective chelators." *Medicinal Research Reviews* 22(1): 26-64.
- Loscher, W. and Potschka, H. (2005). "Blood-brain barrier active efflux transporters: ATP-binding cassette gene family." *NeuroRx : the journal of the American Society for Experimental NeuroTherapeutics* 2(1): 86-98.
- Loscher, W. and Potschka, H. (2005). "Drug resistance in brain diseases and the role of drug efflux transporters." *Nature reviews. Neuroscience* 6(8): 591-602.

- 
- Ma, Y. M. and Hider, R. C. (2010). "Design and synthesis of fluorine-substituted 3-hydroxypyridin-4-ones." *Tetrahedron Letters* 51(40): 5230-5233.
- Mensch, J., Oyarzabal, J., Mackie, C. and Augustijns, P. (2009). "In vivo, in vitro and in silico methods for small molecule transfer across the BBB." *Journal of pharmaceutical sciences* 98(12): 4429-4468.
- Molina-Holgado, F., Hider, R. C., Gaeta, A., Williams, R. and Francis, P. (2007). "Metals ions and neurodegeneration." *Biomaterials* 20(3-4): 639-654.
- Mosmann, T. (1983). "Rapid colorimetric assay for cellular growth and survival: application to proliferation and cytotoxicity assays." *Journal of Immunological Methods* 65(1-2): 55-63.
- Nakagawa, S., Deli, M. A., Kawaguchi, H., Shimizudani, T., Shimono, T., Kittel, A., Tanaka, K. and Niwa, M. (2009). "A new blood-brain barrier model using primary rat brain endothelial cells, pericytes and astrocytes." *Neurochemistry international* 54(3-4): 253-263.
- Nakagawa, S., Deli, M. A., Nakao, S., Honda, M., Hayashi, K., Nakaoke, R., Kataoka, Y. and Niwa, M. (2007). "Pericytes from brain microvessels strengthen the barrier integrity in primary cultures of rat brain endothelial cells." *Cellular and molecular neurobiology* 27(6): 687-694.
- Perriere, N., Demeuse, P., Garcia, E., Regina, A., Debray, M., Andreux, J. P., Couvreur, P., Scherrmann, J. M., Temsamani, J., Couraud, P. O., Deli, M. A. and Roux, F. (2005). "Puromycin-based purification of rat brain capillary endothelial cell cultures. Effect on the expression of blood-brain barrier-specific properties." *Journal of neurochemistry* 93(2): 279-289.
- Persidsky, Y., Ramirez, S. H., Haorah, J. and Kanmogne, G. D. (2006). "Blood-brain barrier: structural components and function under physiologic and pathologic conditions." *Journal of neuroimmune pharmacology : the official journal of the Society on NeuroImmune Pharmacology* 1(3): 223-236.
- Roy, S. (2009). "Iron Chelator Design: Evaluation of Blood-Brain Barrier Permeability and Neuroprotective Properties." *PhD Thesis*, King's College London.
- Roy, S., Preston, J. E., Hider, R. C. and Ma, Y. M. (2010). "Glucosylated Deferiprone and Its Brain Uptake: Implications for Developing Glucosylated Hydroxypyridinone Analogues Intended to Cross the Blood-Brain Barrier." *Journal of medicinal chemistry* 53(15): 5886-5889.

- 
- Rubin, L. L., Hall, D. E., Porter, S., Barbu, K., Cannon, C., Horner, H. C., Janatpour, M., Liaw, C. W., Manning, K., Morales, J. and et al. (1991). "A cell culture model of the blood-brain barrier." *The Journal of cell biology* 115(6): 1725-1735.
- Salvador, G. A., Uranga, R. M. and Giusto, N. M. (2010). "Iron and mechanisms of neurotoxicity." *International Journal of Alzheimer's Disease* 2011: 720658.
- Schapira, A. H., Bezard, E., Brotchie, J., Calon, F., Collingridge, G. L., Ferger, B., Hengerer, B., Hirsch, E., Jenner, P., Le Novere, N., Obeso, J. A., Schwarzschild, M. A., Spampinato, U. and Davidai, G. (2006). "Novel pharmacological targets for the treatment of Parkinson's disease." *Nature reviews. Drug discovery* 5(10): 845-854.
- Skinner, R. A., Gibson, R. M., Rothwell, N. J., Pinteaux, E. and Penny, J. I. (2009). "Transport of interleukin-1 across cerebromicrovascular endothelial cells." *British Journal of Pharmacology* 156(7): 1115-1123.
- Smith, P. K., Krohn, R. I., Hermanson, G. T., Mallia, A. K., Gartner, F. H., Provenzano, M. D., Fujimoto, E. K., Goeke, N. M., Olson, B. J. and Klenk, D. C. (1985). "Measurement of protein using bicinchoninic acid." *Analytical Biochemistry* 150(1): 76-85.
- Snyder, A. M. and Connor, J. R. (2009). "Iron, the substantia nigra and related neurological disorders." *Biochimica et Biophysica Acta (BBA) - General Subjects* 1790(7): 606-614.
- Tabner, B. J., El-Agnaf, O. M., German, M. J., Fullwood, N. J. and Allsop, D. (2005). "Protein aggregation, metals and oxidative stress in neurodegenerative diseases." *Biochemical Society Transactions* 33(Pt 5): 1082-1086.
- Terry, S., Nie, M., Matter, K. and Balda, M. S. (2010). "Rho signaling and tight junction functions." *Physiology* 25(1): 16-26.
- Weiss, N., Miller, F., Cazaubon, S. and Couraud, P. O. (2009). "The blood-brain barrier in brain homeostasis and neurological diseases." *Biochimica et biophysica acta* 1788(4): 842-857.
- Whitnall, M. and Richardson, D. R. (2006). "Iron: A New Target for Pharmacological Intervention in Neurodegenerative Diseases." *Seminars in Pediatric Neurology* 13(3): 186-197.
- Wilhelm, I., Fazakas, C. and Krizbai, I. A. (2011). "In vitro models of the blood-brain barrier." *Acta neurobiologiae experimentalis* 71(1): 113-128.

- Wolburg, H. and Lippoldt, A. (2002). "Tight junctions of the blood-brain barrier: development, composition and regulation." *Vascular pharmacology* 38(6): 323-337.
- Xiuli, G., Meiyu, G. and Guanhua, D. (2005). "Glucose Transporter 1, Distribution in the Brain and in Neural Disorders: Its Relationship With Transport of Neuroactive Drugs Through the Blood-Brain Barrier." *Biochemical Genetics* 43(3): 175-187.
- Youdim, K. A., Avdeef, A. and Abbott, N. J. (2003). "In vitro trans-monolayer permeability calculations: often forgotten assumptions." *Drug Discov Today* 8(21): 997-1003.
- Zhang, Y., Li, C. S., Ye, Y., Johnson, K., Poe, J., Johnson, S., Bobrowski, W., Garrido, R. and Madhu, C. (2006). "Porcine brain microvessel endothelial cells as an in vitro model to predict in vivo blood-brain barrier permeability." *Drug Metabolism and Disposition* 34(11): 1935-1943.

## 8 CURRICULUM VITAE

**Name:** Katharina Brandner  
**Date of birth:** September 11<sup>th</sup>, 1988  
**Nationality:** Austria  
**Address:** Rennweg 75/2/15  
1030 Wien

### Education

1994 - 1998 Elementary School, 2344 Maria Enzersdorf  
1998 - 2004 Secondary School, BG Bachgasse, 2340 Mödling  
2004 - 2005 Exchange student at Cross Roads High School, Malakoff, Texas (USA)  
2005 - 2006 Secondary School, BG Bachgasse, 2340 Mödling

### Academic Studies

Since October 2006 Diploma Study Pharmacy at the University of Vienna, 1090 Vienna  
Feb 2011-Jul 2011 Erasmus student at King's College London, SE1 1UL  
Diploma thesis "Blood-brain barrier permeability of six 3-hydroxypyridin-4ones *in vitro*"

### Work experience

August 2006 Internship at NÖ Landespensionisten- und Pflegeheim, 2340 Mödling  
September 2007 Internship at Novartis Institutes for BioMedical Research Austria, 1230 Vienna  
September 2008 Internship at Boehringer Ingelheim Regional Center Vienna, 1121 Vienna  
Since March 2008 Employee at Millennium Apotheke, 1200 Vienna

## 9 APPENDIX

### 9.1 HPO standard curves

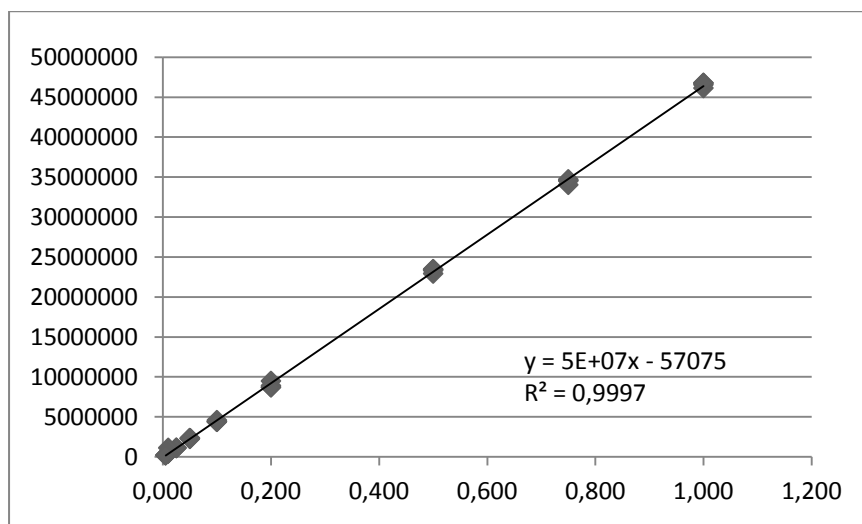


Figure 38: Standard curve CP20

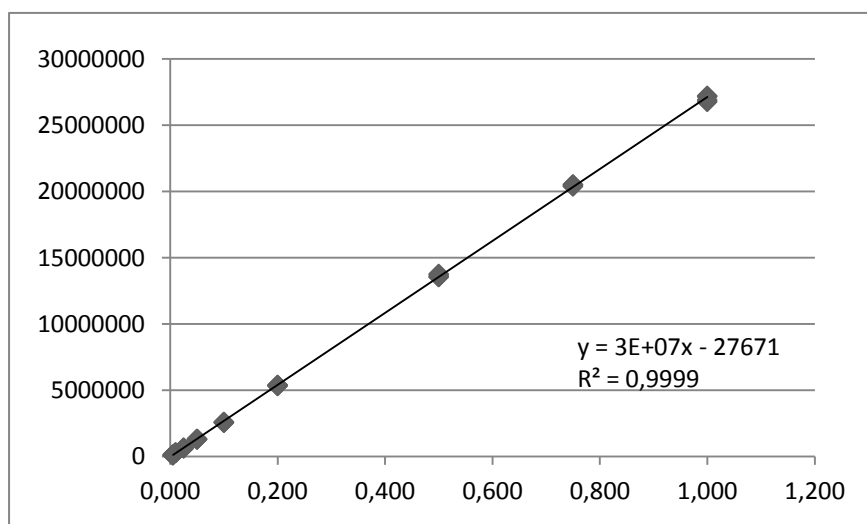


Figure 39: Standard curve YMF 8



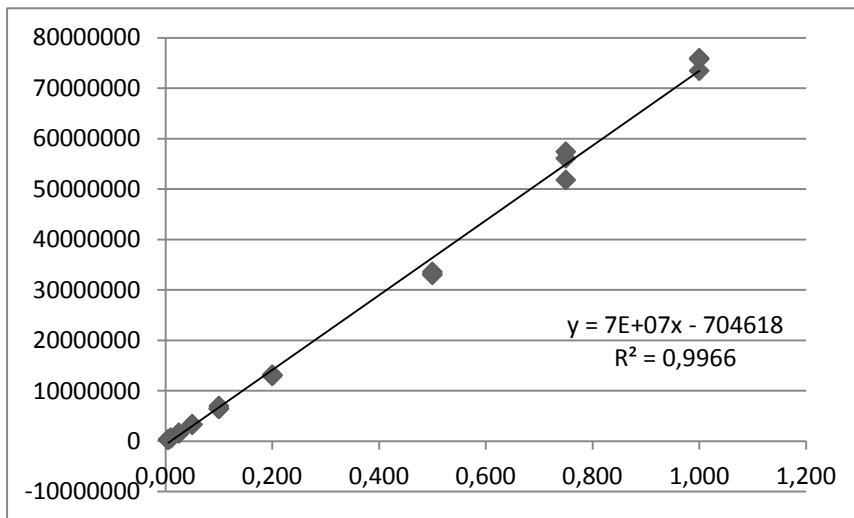


Figure 40: Standard curve YMF 16

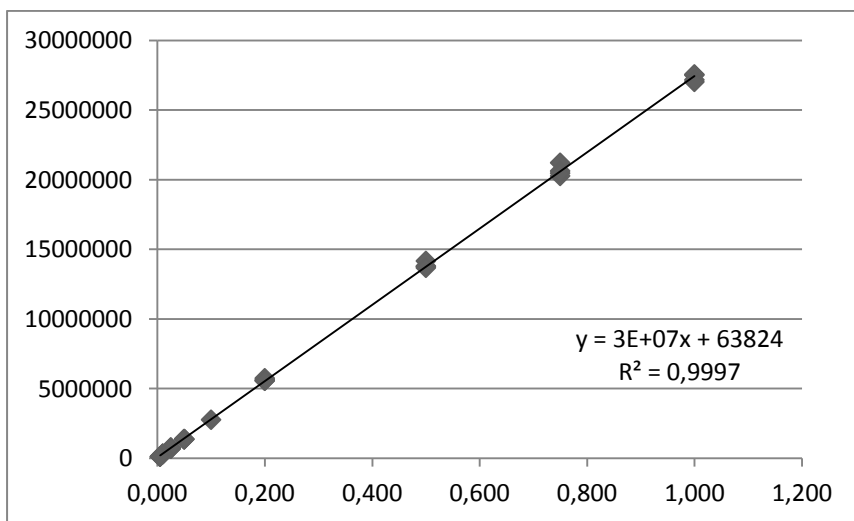


Figure 41: Standard curve YMF 24

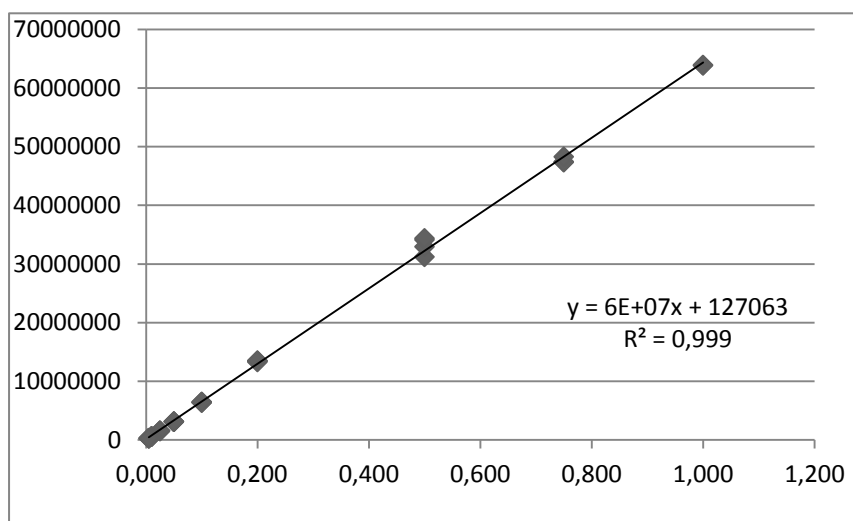


Figure 42: Standard curve YMF 25

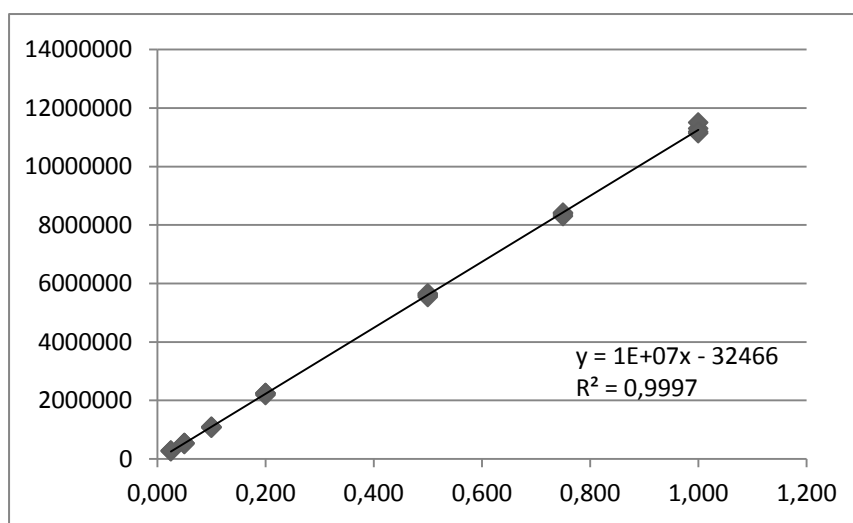


Figure 43: Standard curve YMF 29

## 9.2 HPLC chromatograms

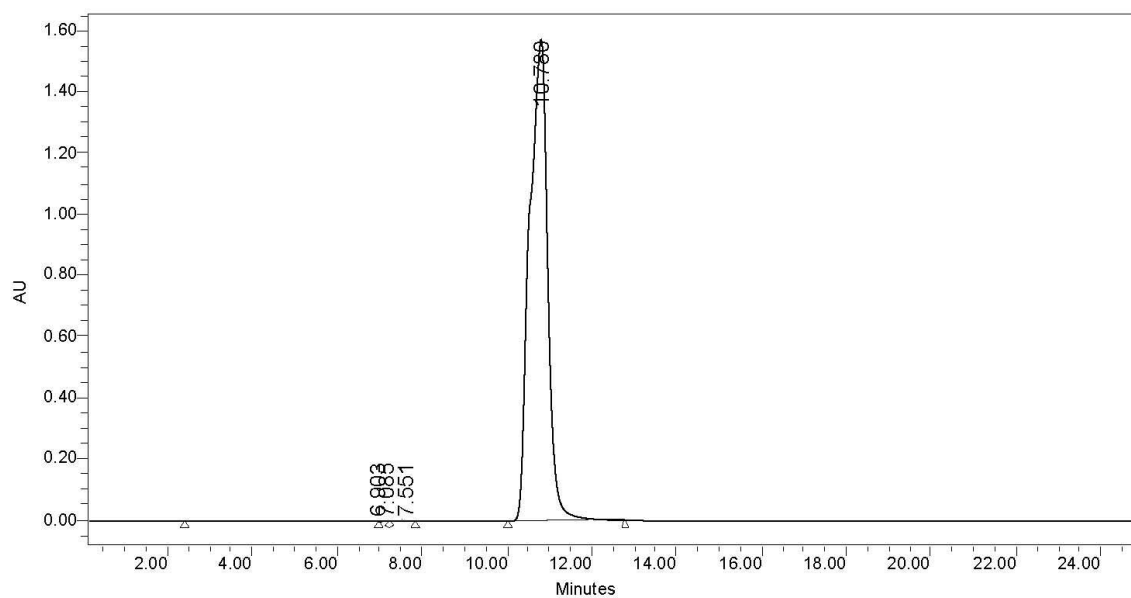


Figure 44: HPLC chromatogram CP20 (1mM), 100µL injection

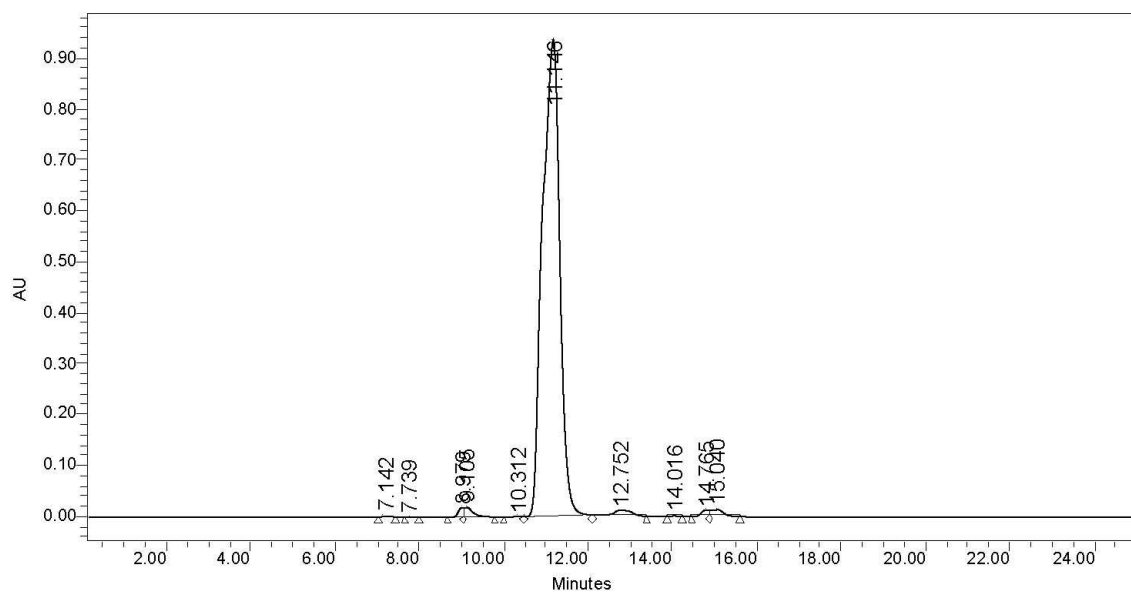


Figure 45: HPLC chromatogram YMF 8 (1mM), 100µL injection

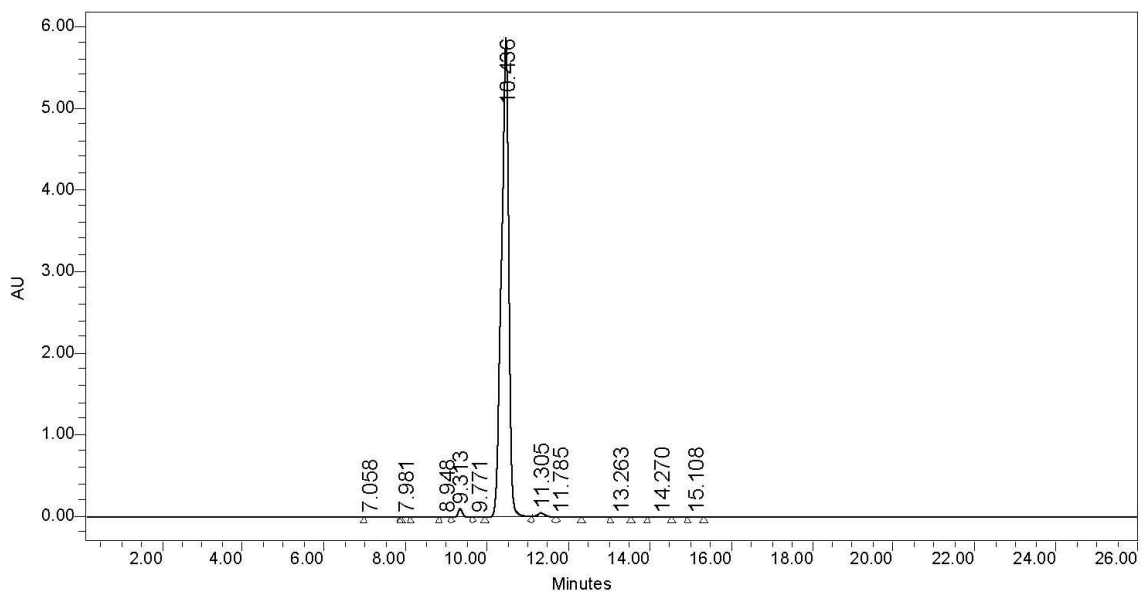


Figure 46: HPLC chromatogram YMF 16 (1mM), 100µL injection

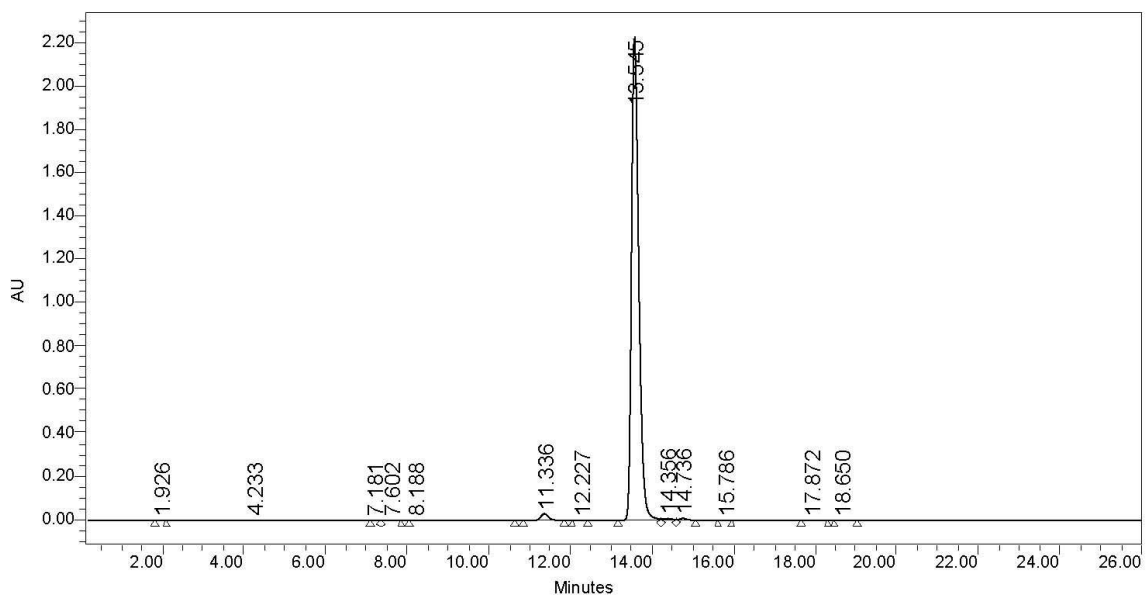


Figure 4726: HPLC chromatogram YMF 24 (1mM), 100µL injection

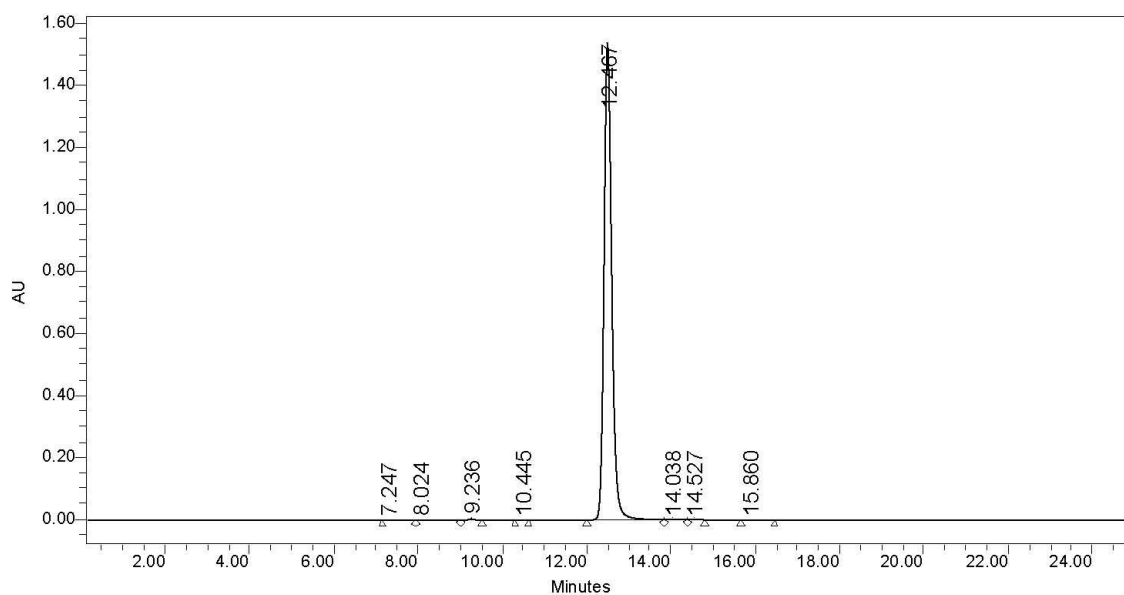


Figure 27: HPLC chromatogram YMF 25 (1mM), 100µL injection

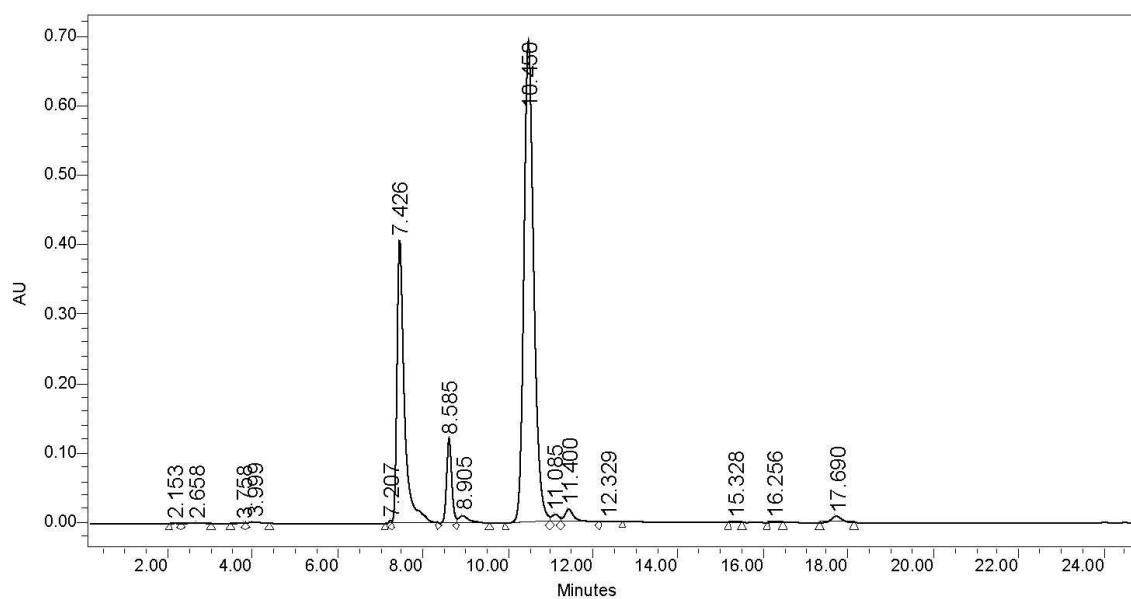


Figure 28: HPLC chromatogram YMF 29 (1mM), 100µL injection

### 9.3 YMF 29 mass spectrometry

M16972 #215-300 RT: 2.05-2.56 AV: 54 NL: 1.88E8  
F: +p ESI Full ms [50.00-500.00]

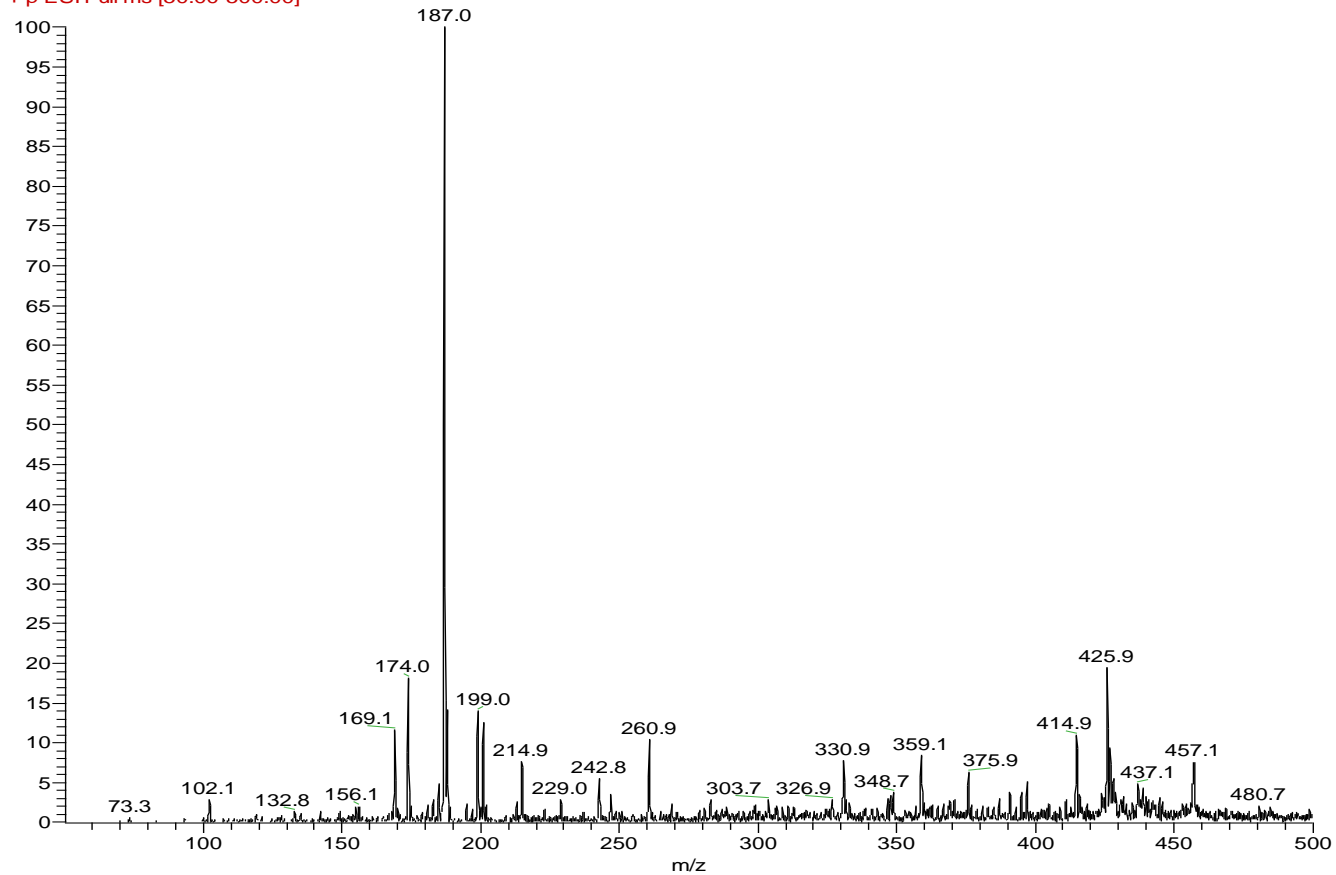


Figure 29: ESI MS(+ve) of YMF 29 (MW 267; YMF 29 – HBr: MW 187), 20 $\mu$ L of sample diluted to 1mL with 0.1% FA in 50% MeOH